PLOS ONE

RESEARCH ARTICLE

Biogenic green synthesis of MgO nanoparticles using *Saussurea costus* biomasses for a comprehensive detection of their antimicrobial, cytotoxicity against MCF-7 breast cancer cells and photocatalysis potentials

Musarat Amina[1]*, Nawal M. Al Musayeib[1], Nawal A. Alarfaj[2], Maha F. El-Tohamy[2], Hesham F. Oraby[3], Gadah A. Al Hamoud[1], Sarah I. Bukhari[4], Nadine M. S. Moubayed[5]

1 Department of Pharmacognosy, Pharmacy College, King Saud University, Riyadh, Saudi Arabia, **2** Department of Chemistry, College of Science, King Saud University, Riyadh, Saudi Arabia, **3** Deanship of Scientific Research, Umm Al-Qura University, Makkah, Saudi Arabia, **4** Department of Pharmaceutics, College of Pharmacy, King Saud University, Riyadh, Saudi Arabia, **5** Department of Botany and Microbiology, College of Science, King Saud University, Riyadh, Saudi Arabia

* mamina@ksu.edu.sa, musarat.org@gmail.com

Citation: Amina M, Al Musayeib NM, Alarfaj NA, El-Tohamy MF, Oraby HF, Al Hamoud GA, et al. (2020) Biogenic green synthesis of MgO nanoparticles using *Saussurea costus* biomasses for a comprehensive detection of their antimicrobial, cytotoxicity against MCF-7 breast cancer cells and photocatalysis potentials. PLoS ONE 15(8): e0237567. https://doi.org/10.1371/journal.pone.0237567

Editor: Yogendra Kumar Mishra, University of Southern Denmark, DENMARK

Received: January 21, 2020

Accepted: July 28, 2020

Published: August 14, 2020

Data Availability Statement: All relevant data are within the paper.

Funding: This research project was supported by a grant from the "Research Center of the Female Scientific and Medical Colleges", Deanship of Scientific Research, King Saud University. The funders had no role in study design, data collection

Abstract

Distinct morphological MgO nanoparticles (MgONPs) were synthesized using biomasses of *Saussurea costus* roots. The biomass of two varieties of *Saussurea costus* (Qustal hindi and Qustal bahri) were used in the green synthesis of MgONPs. The physical and chemical features of nanoparticles were confirmed by spectroscopic and microscopic techniques. The surface morphology of the obtained nanoparticles was detected at different magnifications by SEM and TEM microscopy and the size of nanoparticles were found to be 30 and 34 nm for Qustal hindi and Qustal bahri, respectively. The antimicrobial activity of the prepared MgONPs was screened against six pathogenic strains. The synthesized nanoparticles by Qustal bahri biomass exerted significant inhibition zones 15, 16, 18, 17, 14, and 10 mm against *E. coli*, *P. aeruginosa*, *C. tropicalis* and *C. glabrata*, *S. aureus* and *B. subtilis* as compared to those from Qustal hindi 12, 8 and 17 mm against *B. subtilis*, *E. coli* and *C. tropicalis*, respectively. MgONPs showed a potential cytotoxicity effect against MCF-7 breast cancer cell lines. Cellular investigations of MgONPs revealed that the prepared nanoparticles by Qustal bahri exhibited high cytotoxicity against MCF-7 cancer cell lines. IC_{50} values in MCF-7 cells were found to be 67.3% and 52.1% for MgONPs of *Saussurea costus* biomasses, respectively. Also, the photocatalytic activity of MgONPs of each *Saussurea costus* variety was comparatively studied. They exhibited an enhanced photocatalytic degradation of methylene blue after UV irradiation for 1 h as 92% and 59% for those prepared by Qustal bahri and Qustal hindi, respectively. Outcome of results revealed that the biosynthesized MgONPs showed promising biomedical potentials.

and analysis, decision to publish, or preparation of the manuscript.

Competing interests: The authors have declared that no competing interests exist.

Introduction

Nanomaterials, particularly metal and metal oxide nanoparticles are considered as a unique group of materials with specific physical and chemical features and have wide applications in different scientific fields such as biomedicine [1, 2], biosensing technology [3], catalysis [4, 5], tissue engineering [6], food packaging [7], and environmental sciences [8]. Among all metal oxide nanoparticles, magnesium oxide nanoparticle (MgONPs) has received much attention for its unique biocompatible nature and high stability under extreme conditions [9, 10]. MgONPs have been used in electronics, catalysis, additives, ceramics, photochemical products, paints, and medicine [11, 12]. Conventional procedures for the preparation of MgONPs require toxic chemicals with high amount of external heat and also forms several hazardous side products that could have potential biological and environmental threat. Thus, there always exists a huge desire to develop environmentally compatible, economic, energy efficient green chemical procedures to elude the use of toxic chemicals in the preparation of nanoparticles [13]. To conquer these obstacles, natural products (plants, sponges, and marine algae) presents the excellent resources suitable for the biogenic synthesis of metal and metal oxide nanoparticles. The advantage of using plant biomasses in the synthesis of magnesium oxide nanoparticles is easy accessibility, environment friendly, safe and mostly non-toxic [14]. These herbals contain different types of biomolecules including terpenoids, alkaloids, carboxylic acids and phenolic compounds that can effectively serve as reducing and stabilizing agents in the formation of metal oxide nanoparticles [15]. The *Saussurea costus* (Family Asteraceae) is a perennial or biennial herb naturally found in alpine grassland and on rocky slopes across the northeast and northwest sub Himalayan regions [16]. Literature studies claim that *S. costus* is represented by two varieties; dark brown colored Indian wood costus is known as Qustal hindi and milky white colored sea incense costus is known as Qustal bahri. It is a potent plant used for different medicinal, nutritional and commercial purposes worldwide [17]. In the traditional folk medicine roots of *S. costus* are used as an ethnomedicine to cure indigestion, analgesic, abdominal pain, anthelmintic, dyspepsia, fever, and bronchitis [18]. The extracts and isolated macromolecules of *S. costus* are reported to exhibit antimicrobial [19], anticancer [20], antidiabetic and antilipidemic [21], anti-hepatotoxic [22] and anti-inflammatory [23] properties. Phytochemically, it contains sesquiterpenes, alkaloids, triterpenes, lignans, and tannins as the main bioactive constituents [24].

Over the above described medicinal properties, this plant species has been further used to prepare magnesium oxide nanoparticles due to its immense potential impact in medicine. Consequently, various studies have been carried out on the root extracts of *S. costus*. However, there are no published data available for the utilization of *S. costus* root extract for the synthesis of magnesium oxide nanoparticles. In our study, two varieties of *S. costus* (Qustal hindi and Qustal bahri) root biomasses were utilized for the synthesis of bio and eco-friendly MgO nanoparticles with green chemistry. Magnesium oxide nanoparticles possess astonishing biomedical applications and are used as ointments for the treatment of heart burns, wounds and bone regeneration [25, 26]. Furthermore, these nanoparticles have displayed excellent toxic effects against various multidrug resistant human pathogens and can be used as an alternative medication [27]. The presence of protein caps on the metal oxide nanoparticles contributes in binding and stabilizing the bacterial cell surface, causing increments in binding and absorption of the medicine on infected cells [28]. However, several studies were performed to test the efficacy of magnesium oxide nanoparticles in killing cancerous cells and they were found effective against several cancer cells [29, 30]. Breast cancer is the most common diagnosed cancer among female population taking almost 522,000 lives of women every year worldwide. Despite the modernization in the cancer treatment, complete cure is still a concern [31]. The

conventional treatment of breast cancer revolves around the surgical removal of malignant tissues, chemotherapy, ionizing radiotherapy and hormonal therapy. Unfortunately, all of them induce some severe side effects such as systemic toxicity, high rate of drug resistance and destroying the adjacent normal cells [32]. Hence, there is an urgent demand for alternative strategies to develop ecofriendly, nontoxic, cost effective and targeted drugs to treat the cancer. The unique physico-chemical features of nanomaterial open up new ways for diagnosis and treatment of cancer due to their small size <100 nm, exceptional binding abilities with proteins, lipids and nucleic acids present on the cell surfaces and within the body cells [33]. Currently, metal oxides such as magnesium oxide nanoparticles have been engineered as new useful anticancer therapy tools against various types of cancer [34]. The interaction between magnesium oxide nanoparticles with human serum albumin was addressed and their anticancer activity against leukemia K562 cell line was reported [35]. Moreover, the interaction of magnesium oxide nanoparticles with curcumin and β-cyclodextrin was used as inhibiting agents in the proliferation of breast cancer cells (MCF-7) [36].The combinational treatment of the cancer by magnesium oxide and herbal extracts may cause synergistic cytotoxic effects on the cancer cells.

Considering the medicinal importance of metal oxide nanoparticle synthesis, especially magnesium oxide using different plant extracts, the aim of the current study was green synthesis and characterization of magnesium oxide nanoparticles using *Saussurea costus* root extracts as reducing agents.The biomedical efficacy of MgONPs prepared by two different varieties of *Saussurea costus* (Qustal hindi and Qustal bahri) was individually evaluated for antipathogenic, anticancer and photocatalytic properties.

Material and methods

Botanical and chemical materials

Roots of Qustal hindi (Indian wood Costus) were collected from Kaghan forest (N 33˚ 42' 37.1772, E 73˚ 2.5688 '), while as roots of Qustal bahri (Sea Incense Costus) were collected from a coastal region of Karachi (N 24.7897˚, E 67.0439˚) Pakistan in July 2017, under the supervision of one of the authors (MA). No specific permits were required for field activities including sample collection from the described locations. These locations are open to the public and neither privately owned nor protected in any way. This plant species are very common to the region that does not fall into a category of endangered or protected species as per International Union for the Conservation of Nature (IUNC) rule. These roots were subsequently examined and identified by Prof. Dr. Mohamed Yousef, systematic taxonomist from Department of Pharmacognosy, College of Pharmacy at King Saud University, Saudi Arabia. Voucher specimens bearing catalogue No: (QH-7801) and (QB-7802) were deposited in the herbarium of the same department for Qustal hindi and Qustal bahri, respectively. However, methanol (98.9%, PubChem CID: 887), magnesium nitrate ($Mg(NO_3)_2.6H_2O$, 99.9%), sodium hydroxide (99.8%), and dimethyl sulfoxide (DMSO) were provided by Sigma Aldrich (Hamburg, Germany).

Preparation of *S.costus* biomass

To prepare the *S. costus* biomasses, 1000 g of air-dried, powdered roots of each variety were placed individually in two separate Soxhlet apparatus and extracted by refluxing with 98.9% of methanol (3 L) for 3 h. The whole process was repeated thrice, all the pooled methanolic biomasses was then filtered off and the solvent was removed under reduced pressure on a rotatory evaporator at 50 ^{o}C, affording 345 g and 432 g of methanol biomass for Qustal hindi and Qustal bahri, respectively.

Synthesis of MgO nanoparticles

The synthesis of MgONPs was conducted using two different biomasses of *S. costus*. Briefly, 50 mL of each *S. costus* biomass was mixed with 20 mL (1.0×10^{-3} $molL^{-1}$) of an aqueous solution of $Mg(NO_3)_2$ under continuous magnetic stirring for 4 h at 80˚C. The formation of yellowish brown solution indicated the reduction of $Mg(NO_3)_2$ to MgONPs. Further, the synthesized MgONPs were calcinated for 3 h at 450˚C in a muffle furnace.

Microscopic and spectroscopic characterization

To verify the formation of MgONPs, UV-Vis spectrum was measured in the absorption wavelength ranging from 200 to 800 nm using (UV 2450, Shimadzu, Kanagawa, Japan) spectrophotometer. FTIR-analysis was used to detect and measure the functional group of *S. costus* biomasses used for the preparation of MgONPs in the range of 4000–400 cm^{-1} (PerkinElmer Ltd., Yokohama, Japan). Cu Kα radiation was employed to determine the X-ray diffraction (XRD) spectrum of MgONPs at 40 kV and 30 mA (Siemens, Erfurt, Germany, diffractometer). Scanning Electron Microscopy (SEM) in combination with Energy Dispersive X-ray spectroscopy (model JSM-7610F, JEOL, USA) was used to characterize the surface morphology of biosynthesized MgONPs. Zeta potential (ZP) and dynamic light scattering (DLS) analyzer (dynapro®Plate Reader III, Waytt, Japan) was applied to assess the stability and size of prepared MgONPs.

Antimicrobial activity

Antimicrobial activity of synthesized MgONPs with two different biomasses of *Saussurea costus* (Qustal hindi and Qustal bahri) was measured in terms of zone of inhibition against four bacterial (Gram positive: *Staphylococcus aureus* ATCC 25923 and *Bacillus subtilis* ATCC 6633, Gram negative; *Escherichia coli* ATCC 25966 and *Pseudomonas aeruginosa* ATCC 27853) and two fungal (*Candida tropicalis* ATCC 66019 and *Candida glabrata*) strains using agar well diffusion assay [37]. The bacterial and fungal isolates were pre-cultured on nutrient agar (Oxoid) and PDA (potato dextrose agar, Oxoid). The microbial suspension of 0.5 McFarland turbidity from each microbe was prepared in 5 mL nutrient broth tubes for the antimicrobial assays. The prepared microbial suspensions were loaded on the surface of Mueller Hinton (Oxoid) plates by using sterile cotton swabs. Wells (6 mm) were made on the surface of the agar plates by using sterile cork borer and then each well was loaded with 100 μL of each MgONPs (15–35 μgmL^{-1} DMSO), respectively. Plates were incubated aerobically at 37˚C for 18–24 h.

Bacteriostatic and bactericidal (MIC and MBC) determination

In current study, minimum inhibitory concentration (MIC) of MgONPs against *E. coli* and *P. aeruginosa* was conducted in triplicates by Micro-broth dilution assay. The tested concentrations were ranged from 5 to 1280 $\mu g\ mL^{-1}$. Briefly, 2-fold serial dilutions were performed in 96 well plates where the first column was the positive control (containing the broth and the microbial cells) and the last column as the negative control (broth and the MgONPs). 50 μL of each of the microbial suspensions was loaded, respectively, and after incubation for 24 h at 37˚C the results were recorded at 600 nm using an ELISA reader (Biotech). For comparison, tetracycline (TE, 30 μg) and DMSO were used as a positive and negative control, respectively. The lowest concentration of MgONPs which can cause a complete bactericidal effect (MBC) was measured by plating aliquots of tubes with first turbid and no visible growth. Aliquots of treated samples were uniformly spread on nutrient agar plates using a sterile L rod and incubated for 12 h at 37˚C.

Morphological study of *E. coli* and *P. aeruginosa* (SEM)

Scanning electron microscopy was used to evaluate the effect of MgONPs on the morphology of both treated and untreated *E. coli* and *P. aeruginosa*. Treated bacteria were cut into 5- by 10-mm pieces, fixed in 3% gluteraldehyde in phosphate buffer saline solution for 1 h, followed by fixation in 2% osmium tetroxide for another 1 h. The tissues were then dehydrated in ethanol and dried with carbon dioxide. The dried tissues were mounted on aluminum stubs with silver pain vacuum coated with gold palladium alloy and viewed by SEM at an accelerating voltage of 15 kV.

Cytotoxicity of green biosynthesized MgONPs

Human breast cancer line MCF-7 was purchased from the Research Center of King Faisal Specialist Hospital, Saudi Arabia and cells were grown as monolayer cultures maintained in Dulbecco's Modified Eagle Media (DMEM) with 10% Fetal Calf Serum, 100 U/mL of Penicillin G, 50 μgmL^{-1} of Gentamycin and 100 μgmL^{-1} of Streptomycin at 37˚C in a humidified atmosphere with 5% CO_2. DMSO was used to prepare the stock solution and kept in refrigerator at −20˚C till further use. In this study, freshly prepared aliquots with 0.1% in DMSO were used at a final concentration and measurements were performed in triplicates. The cytotoxicity of biosynthesized MgONPs was evaluated by MTT and LDH assays. Briefly, the succinate dehydrogenase enzyme released from mitochondria of live cell cleaved tetrazolium rings of 3-[4,5-dimethylthiazol-2- yl]-2,5-diphenyl tetrazolium bromide (MTT) and viable cells turned yellowish MTT solution into violet colored formazan crystals. This assay is reliable, sensitive, and quantitative method for the measurement of cell viability [38]. Each well of 96-well plate was seeded by 100 μL of MCF-7 cell solution in freshly prepared media with cell density of 1.0×10^4 cells mL^{-1} and incubated for 12 h. After incubation, equal amount of fresh medium was used to replace the supernatant of old culture media and incubated for 48 h after adding different concentrations (20, 40, 60, 80 and 100 μgmL^{-1}) of MgONPs (Qustal hindi and Qustal bahri). After the appropriate incubation, 100 μL MTT solution (0.5 $mgmL^{-1}$) was added to each plate and kept in the dark at 37˚C for 4 h. The cells in the plate were finally centrifuged at 800 rpm for 3 min and the supernatant was replaced by 100 μL of DMSO containing violet colored-formazan crystal. Then, the microtiter plate reader was used to record the absorbance at 570 nm. The cell viability percentage was calculated using the following equation: Cell viability % = (OD of the treated MgONPs cells/ OD of the untreated cells) × 100, and then IC_{50} was calculated [39]. Additionally, lactate dehydrogenase leakage (LDH) assay was used to assess the damage of cell membrane and loss of membrane integrity [40]. The qualitative and quantitative analysis of intracellular reactive oxygen species (ROS) was carried out according to Laurite et al. method [41] by using fluorescent probe DCFH-DA at emission wavelength 540 nm after excitation at 487 nm. However, the potential changes in mitochondrial membrane ($\Delta\Psi m$) after the treatment with MgONPs were determined by Suganthy et al [42] method by using Rhodamine 123 staining.

DNA fragmentation detection

8 well plates were seeded with 1.0×10^5 MCF-7 cells and incubated for one day. After changing the culture medium with freshly prepared medium, MgONPs was added at IC_{50} concentration values as a test drug. Paclitaxel and 1X phosphate buffer saline of pH 7.4 were used as a control for positive and negative groups, respectively. Further incubation was performed under humidified air with 5% CO_2 in one day at 37˚C. The DNA was isolated from the harvested cells and dissolved separately in the DNA loading buffer. The electrophoresis was carried on 1.5% agarose gel [43].

Apoptosis of MCF-7 cells

Double staining with two dyes, acridine orange (AO) and ethidinum bromide (EtBr) was used to facile the estimation of cancer cell death. Following MgONPs treatment, MCF-7 cells were washed with phosphate buffer solution and stained with an AO/EtBr solution (1:1, v/v) at a final concentration of 200 μgmL^{-1} and incubated for 30 min. The first dye destroys the cell membrane and binds with the nucleic acid of the cell and emits green fluorescence while the second dye can enter the cell after membrane destruction and binds with the nucleic acid to produce red fluorescence [38].

The detection method was conducted by seeding MCF-7 cells of 1.0×10^4 cells into each well plate and incubated for one day. After replacing the old culture medium with new freshly prepared, 200 μL of the medium was kept and the synthesized MgONPs in IC_{50} concentration values was added. 20 to 100 μg/mL^{-1} solution of MgONPs was prepared in DMEM medium. Different concentrations have been tried in order to find out the minimum inhibitory concentration. In earlier reported literature the MgO nanoparticles (200μg) were found effective against lung cancer cell line A549 [44]. So considering the previous study, we selected the above mentioned concentrations in order to find out IC_{50} values. Paclitaxel and 1X phosphate buffer saline of pH 7.4 were used as a control for positive and negative groups, respectively. Further incubation was performed under humidified air with 5% CO_2 in one day at 37˚C, then the culture medium was removed and phosphate buffer saline (1.0×10^{-3} mol L^{-1}, pH 7.4) was used to wash the cancer cells. The cells were kept in the dark after staining by 100 μg mL^{-1} of each AO and EtBr and incubated for 30 min. Then the cells were detected under an inverted microscope (blue filter fluorescence) at 400 x magnification, after washing with phosphate buffer saline (1.0×10^{-3} mol L^{-1}, pH 7.4) [45]. The 40-6-diamidino-2-phenylindole (DAPI) stain was used to study the nuclear morphology of MCF-7 cancer cells by forming double-stranded DNA fluorescent complexes [46]. The nuclear morphology detection was carried out using fluorescence blue filter under inverted microscope after adjusting the cell conditions. Briefly, each well was seeded with 1.0×10^4 MCF-7 cells and incubated for one complete day. The same procedure as mentioned above was followed using DAPI staining after washing the cells with phosphate buffer saline (1.0×10^{-3} mol L^{-1}, pH 7.4) [47].

Scratch wound healing assay

8-well plate was seeded with MFC-7 cells at 1.0×10^4 cells/mL concentration after growing to 80% and harvested by trysinization. The seeded well plates were incubated in Dulbecco's Modified Eagle Medium (DMEM) for one day at 37˚C. The fresh medium without fetal bovine serum was used to replace the culture medium and incubated further for one day. In the center of each well, which contains monolayer cancer cells, a scratch wound was made with a sterile pipette tip (10 mL) and washed three times with 10 mM phosphate buffer saline. The wounded cells were administrated with 1 mL of complete medium and MgONPs were given to the test group and medium was used as control followed by incubation at different time intervals (24, 48 and 72 h). An inverted microscope was used to take the images of migrated cells at 100 x magnification [48].

Catalytic activity of MgONPs

The ability to degrade the methylene blue dye in the presence of visible and ultra-violet radiations, the catalytic activity of the biosynthesized MgONPs nanoparticles was tested. About 25 mg of MgONPs were mixed with 250 mL of methylene blue dye solution under continuous magnetic stirring in dark for 30 min. After equilibrium between the tested dye and MgONPs was achieved, the mixture exposed to sunlight and UV radiation using 120 W mercury vapor

lamp. After regular time intervals (20 min), 5 mL of the suspensions was withdrawn and centrifuged. The UV–visible spectrophotometer (Biotek, Elx 50, Canada) was used to measure absorbance at 660 nm and percentage rate of degradation e of the dye was calculated as per the formula:

$$\%\ \text{of degradation} = C_i\text{–}C_f/C_i \times 100$$ where, C_i and C_f were the initial and final concentrations of dye at a time interval t respectively.

Statistical analysis

Statistical analyses were carried out in triplicates using one-way ANOVA and the data were expressed as mean ± Standard deviation at the degree of confidence limit p value < 0.05.

Results and discussion

Spectroscopic analysis

The synthesis of MgONPs was confirmed by UV-Vis technique (Fig 1A). The size, shape and the nanoparticles distribution in the colloidal matrix influences the surface plasmon resonance (SPR) band [49]. The appearance of SPR band at wavelengths lesser than 300 nm revealed the presence of tiny particles, however at longer wavelengths, proved the presence of anisotropic nanoparticles [50]. In the current study the color transition from yellow to yellowish brown and dark brown revealed the formation of MgONPs from $Mg(NO_3)_2$ by using biomass of two varieties of *S. costus* (Qustal hindi and Qustal bahri). Two different sharp absorption peaks were observed at the same wavelength at 250 and 320 nm for MgONPs of *Saussurea costus* biomasses (Qustal hindi and Qustal bahri). The appearance of absorption peaks at these wavelengths confirmed the formation of small sized MgONPs as previously addressed by Nakamoto [51] and Sharma et al [52]. The difference in the absorption intensities of the yellow to brown color (conformation for MgONPs formation) indicated the variation in effective reduction of the metallic magnesium oxide by different *Saussurea costus* biomasses referring to their reducing capabilities. It is a well-known fact that MgONPs exhibit various colors according to their size and morphology [53]. From Fig 1A, the intense and sharp SPR peak was observed for MgONPs synthesized using Qustal bahri biomass and the increase in intensity of the absorption band is attributed to the formation of a large number of highly dense nanoparticles [54]. It was noticed that the size and distribution of the synthesized magnesium oxide nanoparticles were highly influenced by the type of biomass used [55]. Additionally, the other absorption peak in 200–250 range revealed the presence the various bioactive constituents such as polyphenolics and flavonoids, which might be accountable for the $Mg(NO_3)_2$ reduction to MgONPs.

FTIR analysis was performed to identify the bioactive constituents of green synthesized MgONPs using *Saussurea costus* (Qustal hindi and Qustal bahri). As shown in Fig 1B (1a and 1b), FTIR profile of MgONPs displayed six main bands assigned to different bioactive functional groups. The bands at 3432 (OH stretching), 1402 (OH bending vibration), 1624 ((C = O)NH group), 2918 (C-H aromatic stretching), 1056 (C = O stretching) and 661(Mg-O stretching) cm^{-1} were displayed by MgONPs prepared by Qustal hindi. However, the bands at 3432 (OH stretching), 1462 (OH bending vibration), 1634 ((C = O)NH group), 2918 (C-H aromatic stretching), 1165 (C = O stretching) and 594 (Mg-O stretching) cm^{-1} were displayed by MgONPs prepared by Qustal bahri [56]. The similarity between the spectra of two varieties of magnesium oxide nanoparticles (Qustal hindi and Qustal bahri) show some marginal shifts in peak position and the absence of some peaks, clearly indicate the presence of residual plant biomass in the reduction matrix. The shift in the peaks with low

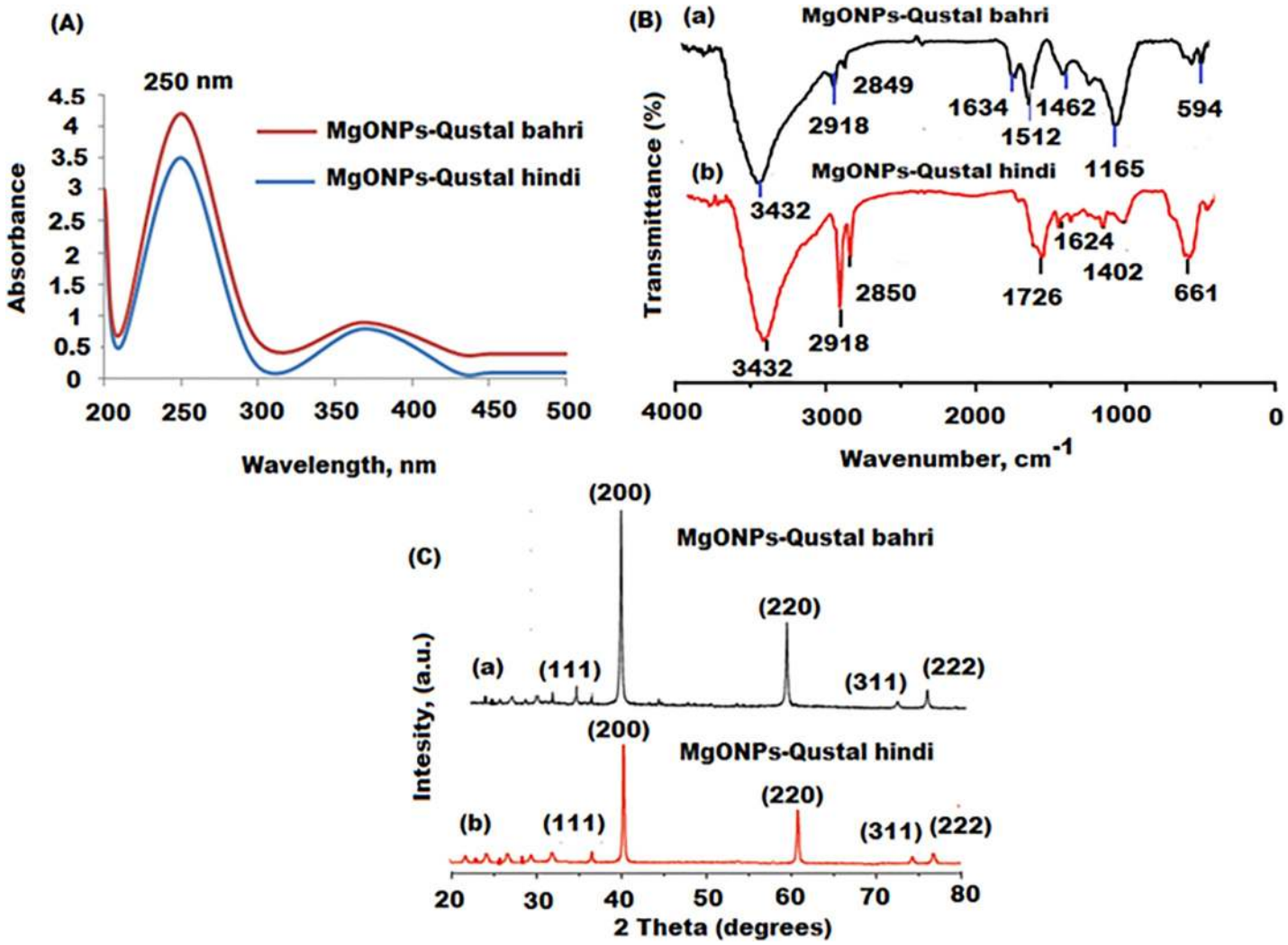

Fig 1. (A) UV-Vis, (B) FT-IR and (C) XRD spectra of MgONPs synthesized with *S.costus* (Qustal hindi and Qustal bahri) biomasses, respectively.

https://doi.org/10.1371/journal.pone.0237567.g001

band intensity were observed in the frequency near 1402, 1624, 1056 and 594 cm^{-1} implying that hydroxyl, (C = O)NH, C = O, and Mg-O groups from the Qustal bahri biomass were more capped with magnesium oxide nanoparticles [55]. The variations in the FTIR spectrum in two above titled MgONPs could be due the presence of different types of chemical constituents of *S. costus* (Qustal hindi and Qustal bahri) biomasses. Thus, the FTIR analysis can be used to confirm the bending and stretching vibrational frequency of MgONPs and the obtained results suggested that the phenolics and flavonoids present in biomasses of *Saussurea costus* (Qustal hindi and Qustal bahri) might be responsible for the formation of MgONPs from the reduction of $Mg(NO_3)_2$.

The XRD-analysis was used to characterize the nano and crystal structure of MgONPs. At optimal conditions the XRD pattern of MgONPs showed five significant peaks at 37.28˚, 41.82˚, 61.25˚, 74.65˚, and 77.45˚ representing 111, 200, 220, 311 and 222 planes, respectively (Fig 1C, a and b). The XRD pattern revealed that the synthesized MgONPs were cubic in structure and crystalline in nature (JCPDS file no. 39–7746) with particle size around 30 nm and 34 nm for Qustal hindi and Qustal bahri, respectively. Almost similar XRD results were reported for MgONPs prepared by other biogenic materials [44].

Microscopic analysis

The TEM and SEM images illustrate the shape and size of green synthesized MgONPs prepared by two varieties of *Saussurea costus* (Qustal hindi and Qustal bahri) at different magnifications (250000x and 80000x). Fig 2A and 2B showed a well dispersed and face centered cubic particles. However, SEM images gave further insight of their size and shape confirming that the surface morphology of MgONPs were uniformly distributed as cubic shaped assemblies of nanoparticles with particle size around 34 and 30 nm (Fig 2C and 2D).

The EDS analysis showed prominent signals corresponding to Mg and O elements confirming the formation of MgONPs (Fig 3A, 3A and 3B). The results indicated that the average percentages of Mg and O were 38.15, 27.92 and 85.23, 86.01 for MgONPs prepared from *S. costus* (Qustal hindi and Qustal bahri), respectively. The dynamic light scattering (DLS) analyzer was used to assess the size and dispersion of the green synthesized MgONPs [57]. The calculated size of nanostructures ranged between 60–100 and 20–50 nm for MgONPs suspensions

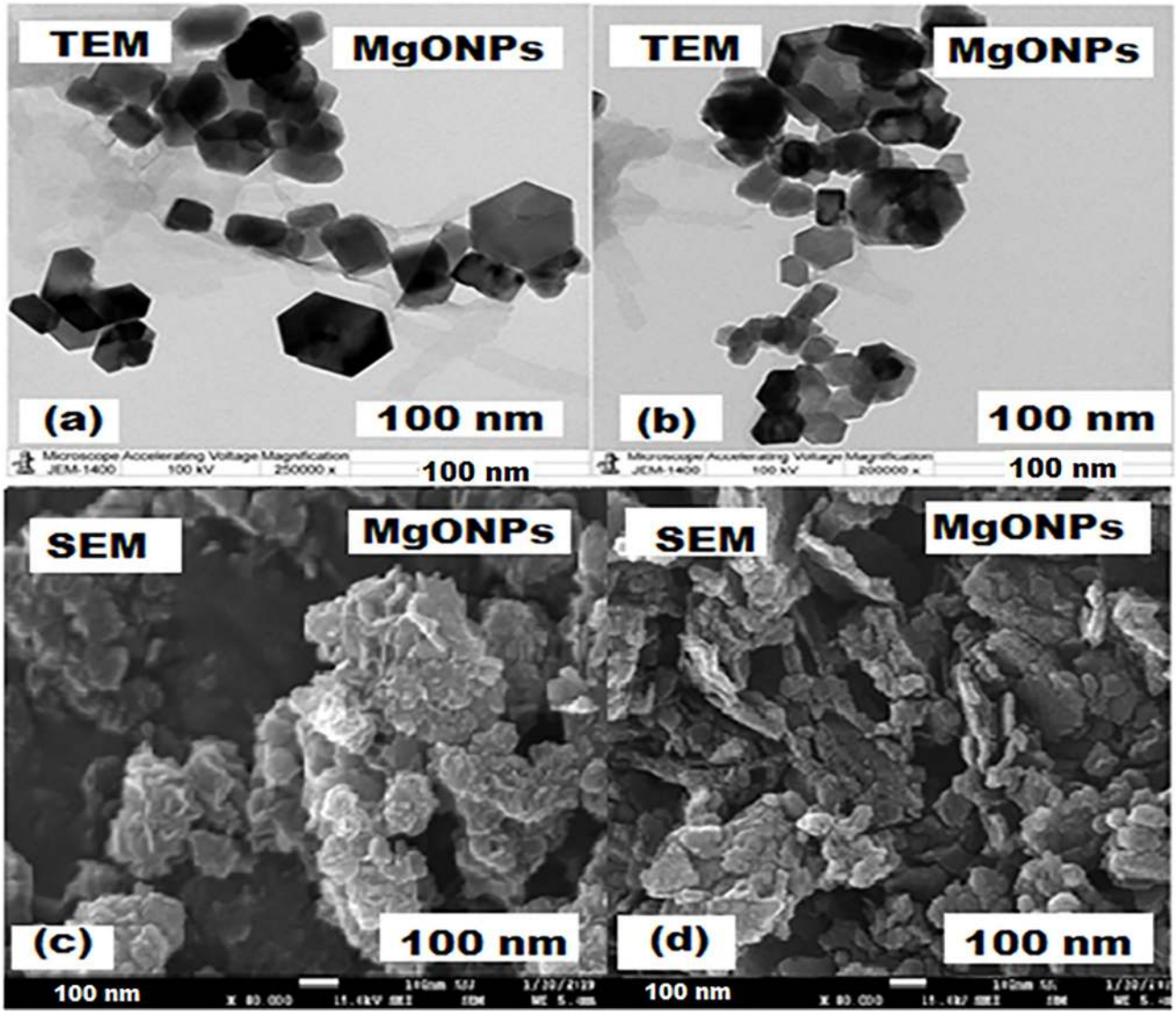

Fig 2. (a and b), (c and d) are the TEM and SEM images of MgONPs synthesized by *S.costus* (Qustal hindi and Qustal bahri) biomasses, respectively.

https://doi.org/10.1371/journal.pone.0237567.g002

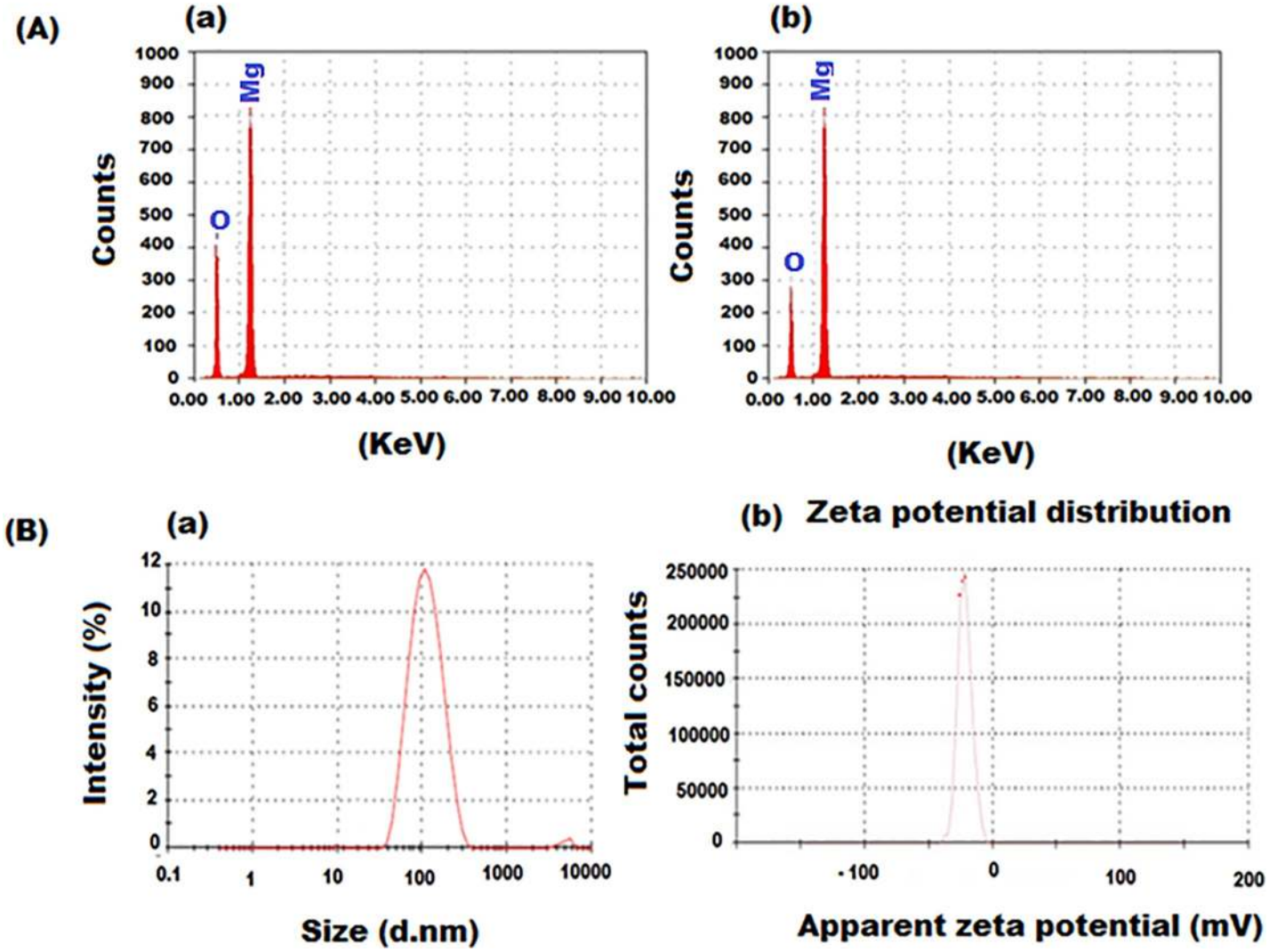

Fig 3. (A) EDS analysis (B) DLS and Zeta potential of MgONPs synthesized by *S.costus* (Qustal hindi and Qustal bahri), respectively.

https://doi.org/10.1371/journal.pone.0237567.g003

prepared by Qustal hindi and Qustal bahri, respectively with PDI (Poly dispesity index) of 1.00. The presence of the single peak conformed that the quality of biosynthesized MgONPs was excellent (Fig 3B and 3A). The observation can be accredited to the difference in concentration and combination of molecules present in the biomasses were the x-factor for the synthesis of different MgONPs. Zeta potential (ZP) determination is based on disturbance of nanparticles under the effect of electrostatic force and their environment. The formation of MgONPs was resulted form hydrogen bond and electrostatic interaction of biomolecules capping magnesium oxide [55]. There is no direct interaction between the nanoparticles even in accumulated conditions, suggesting their stability is due to capping metal oxide. The stability of prepared MgONPs was measured by zeta potential (ZP) and the results showed a high negative potential value of -20.5 mV indicating that the synthesized MgONPs are highly stable (Fig 3B and 3B).

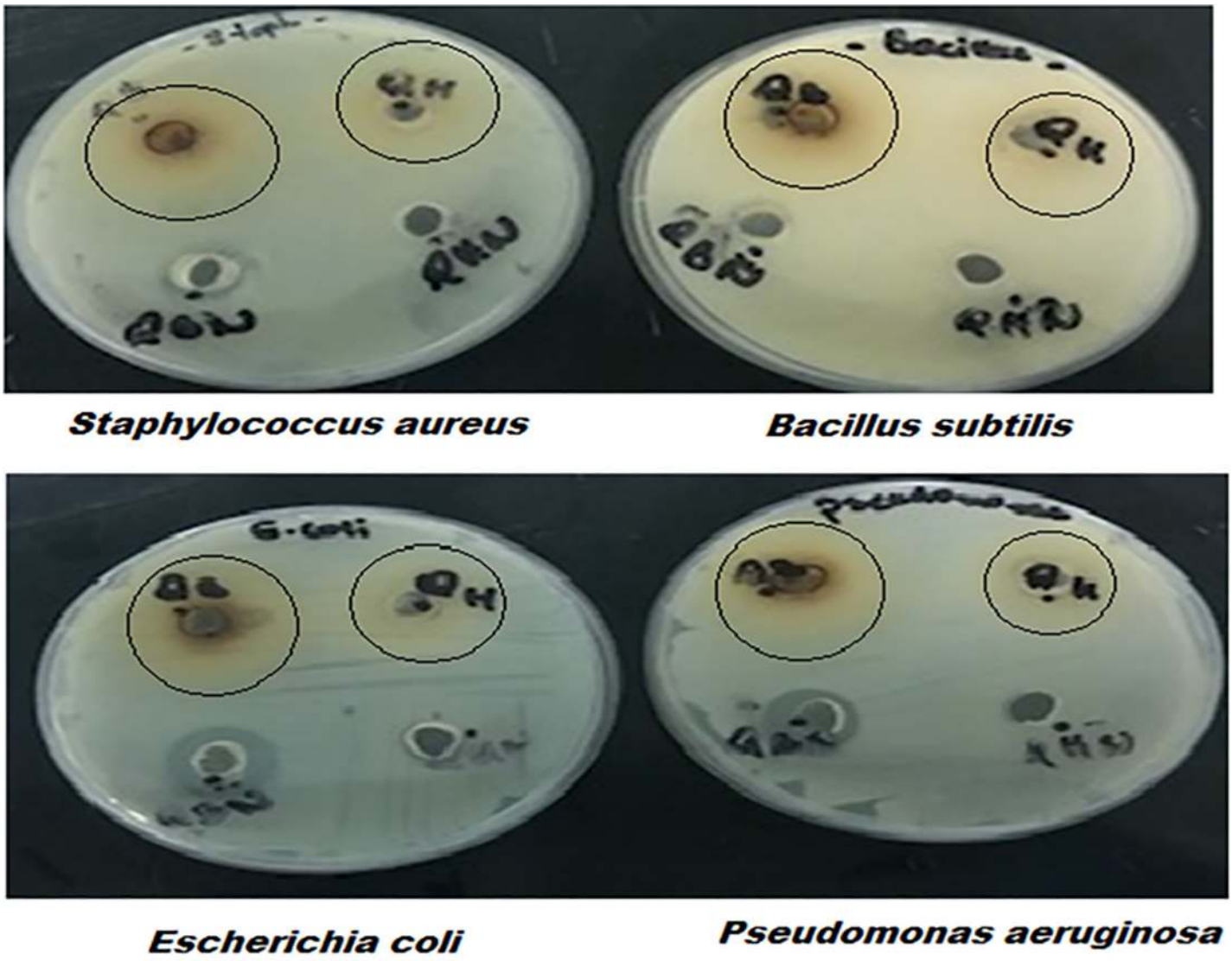

Fig 4. Antimicrobial activity of MgONPs synthesized by *S. costus* (Qustal hindi and Qustal bahri) against four bacterial strains.

https://doi.org/10.1371/journal.pone.0237567.g004

Antimicrobial activity

Antibacterial. The antibacterial effect of green synthesized MgONPs with *S. costus* (Qustal hindi and Qustal bahri) were investigated and the obtained results demonstrated that MgONPs exerted potent antibacterial activity in a dose dependent manner (Fig 4 and Table 1).

Table 1. Antibacterial activity MgONPs prepared from *S. costus* (Qustal hindi and Qustal bahri) against gram positive and gram negative bacteria.

Microorganisms	Zone of inhibition (mm) at conc. μg mL^{-1}						
	MgONPs (Qustal hindi)			MgONPs (Qustal bahri)			Positive control
	15	25	35	15	25	35	
S. aureus	-	-	-	11	11	14	19
B. subtilis	9	10	17	9	10	10	12
E. coli	-	8	8	14	15	15	15
P. aeruginosa	-	-	-	12	13	16	16

https://doi.org/10.1371/journal.pone.0237567.t001

The inhibition zones were obtained as *E. coli* (15 mm), *P. aeruginosa* (16 mm), *S. aureus* (14 mm) and *B. subtilis* (10 mm) for MgONPs prepared from Qustal bahri. However, the inhibition zones obtained from MgONPs prepared by Qustal hindi were effective against *E. coli*, and *B. subtilis* as 8, and 12 mm, respectively. Thus, the above results indicated that the MgONPs synthesized by Qustal bahri showed excellent antibacterial activity against all tested pathogens rather than those obtained from MgONPs prepared Qustal hindi and the highest activity was observed against *E. coli* and *P. aeruginosa* at a concentration 35 μg mL^{-1}. Furthermore, this higher antibacterial activity of synthesized MgONPs (Qustal bahri) can be attributed to their small size, morphology as well as the nature of bioactive compounds present in the *Saussurea costus* biomass.

MIC and MBC of MgONPs against *E. coli* and *P. aeruginosa*. Agar well diffusion method was used to access the bacteriostatic and bactericidal concentration of MgONPs. The minimum concentration required to inhibit the visible growth of *E. coli* and *P. aeruginosa* was determined after incubation at 37˚C for 24 h. The increase of MgONPs concentration (5–1280 μg mL^{-1}) resulted in significant reduction in bacterial cell viability ($p < 0.05$). MIC for *E. coli* and *P. aeruginosa* was 320 μg mL^{-1} (Fig 5A and 5B). MBC is the lowest concentration of test compound that causes death of bacterium under certain specific condition within a fixed time period [58]. MBC for *E. coli* and *P. aeruginosa* was observed 320 and 1280 μg/ml of MgONPs, respectively (Table 2). The bactericidal effect of MgONPs such as cell and membrane damage might be attributed to oxidative stress induced by spontaneous release of ROS and RNS free radicals or electrochemical interaction between LPS with Mg^{2+} ions (Scheme 1) [59]. The observed zones inhibition could be related to the penetration of nanoparticles to the bacterial cells, preventing their growth.

Morphological study of *E. coli* and *P. aeruginosa* (SEM). The effect of MgONPs on the surface morphology of *E. coli* and *P. aeruginosa* was examined under SEM. As shown in Fig 6C and 6F the size and shape of the selected bacteria was changed when treated with MgONPs as a result of the surface coating of bacterial cells by nanoparticles. MgONPs penetrate the peptidoglycan membrane of *E. coli* and *P. aeruginosa* causing its damage, releasing the cell contents and consequently leading to cell death [59]. These results were compared with untreated bacterial cells (Fig 6A and 6D).

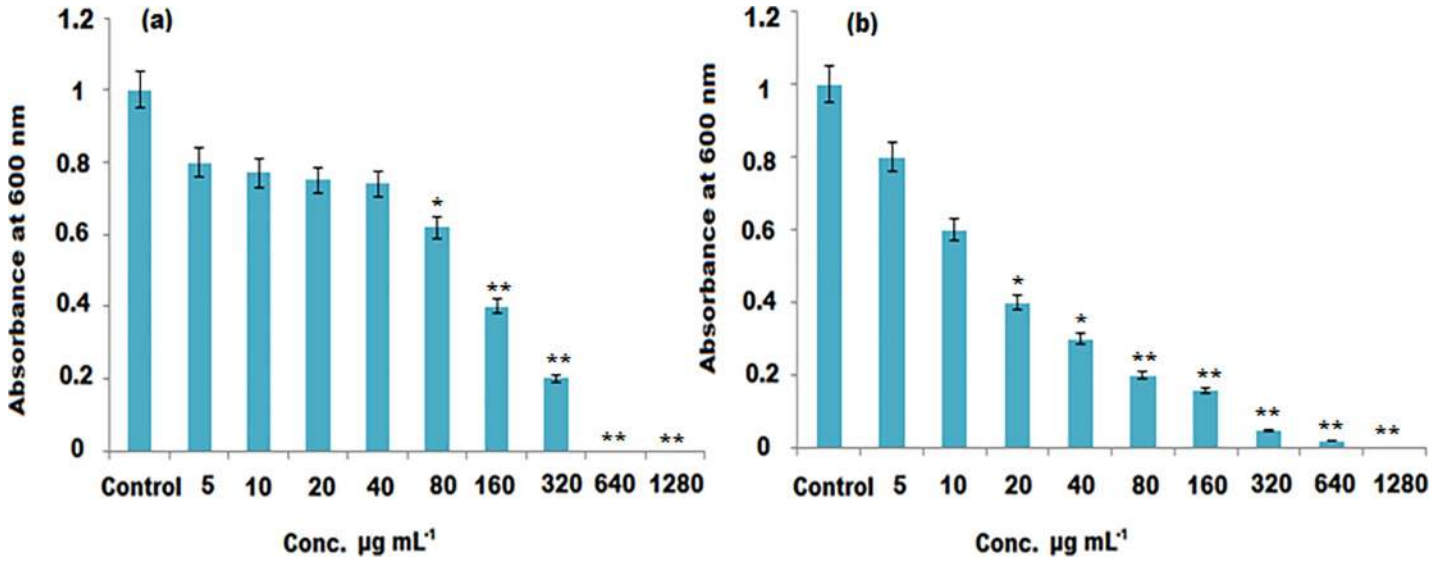

Fig 5. Minimum bactericidal concentrations (μg mL^{-1}) of the MgONPs (Qustal bahri) against (a) *E. coli* (b) *P. aeruginosa*. Results are expressed as Mean ± SD of triplicate experiments.

https://doi.org/10.1371/journal.pone.0237567.g005

Table 2. Minimum bacetericidal activity of MgONPs (Qustal bahri) against *E. coli* and *P. aeruginosa*.

Sample	CFU mL^{-1}	
	E. Coli	*P. aeruoginosa*
Control	TNTC	TNTC
5	TNTC	TNTC
10	TNTC	TNTC
20	TNTC	TNTC
40	TNTC	TNTC
80	TNTC	TNTC
160	2×10^2	4×10^4
320	135	2×10^2
640	5	NIL
1280	1	NIL

https://doi.org/10.1371/journal.pone.0237567.t002

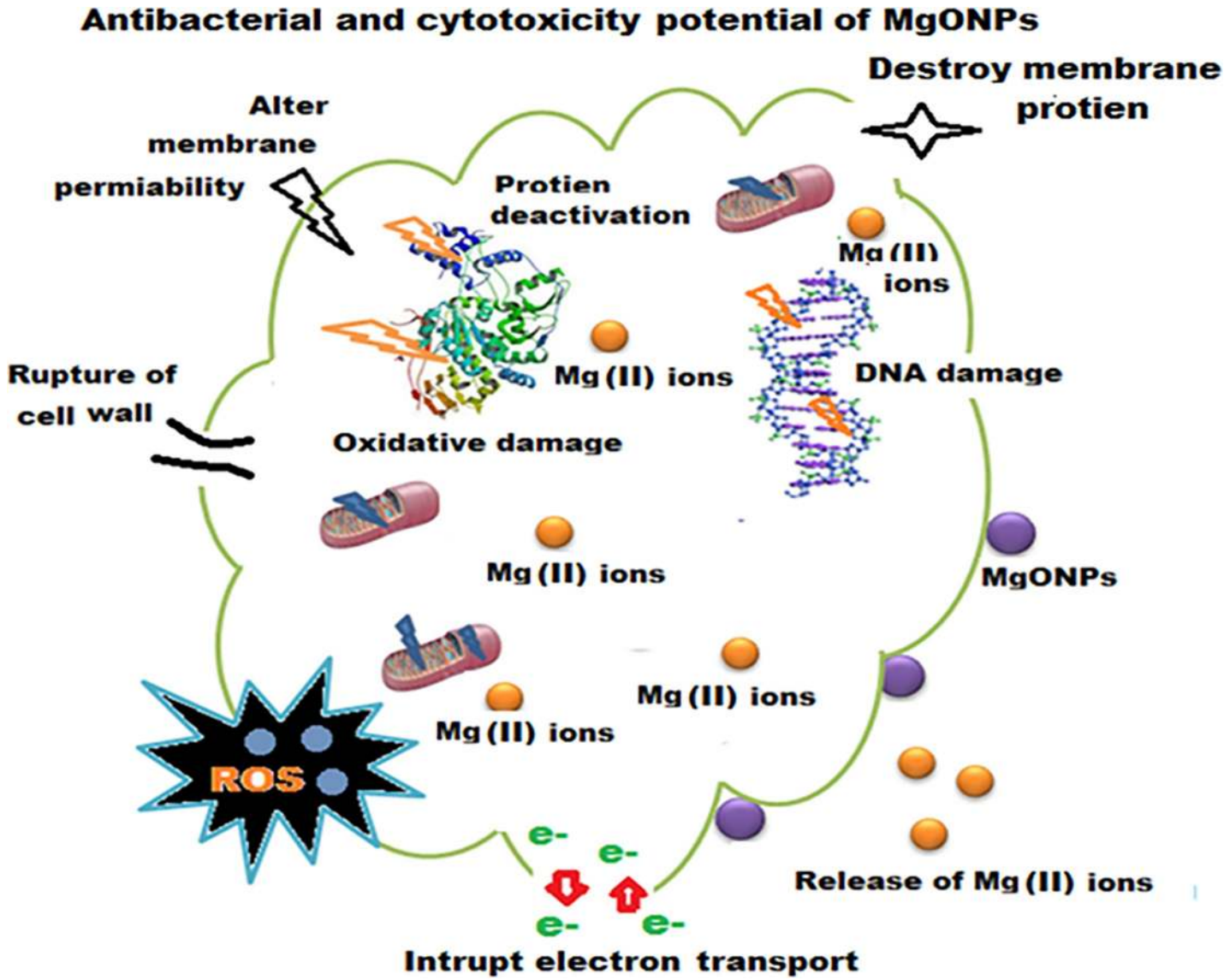

Scheme 1. Schematic diagram of the mechanism of antibacterial and cytotoxicity potential of MgONPs.

https://doi.org/10.1371/journal.pone.0237567.g006

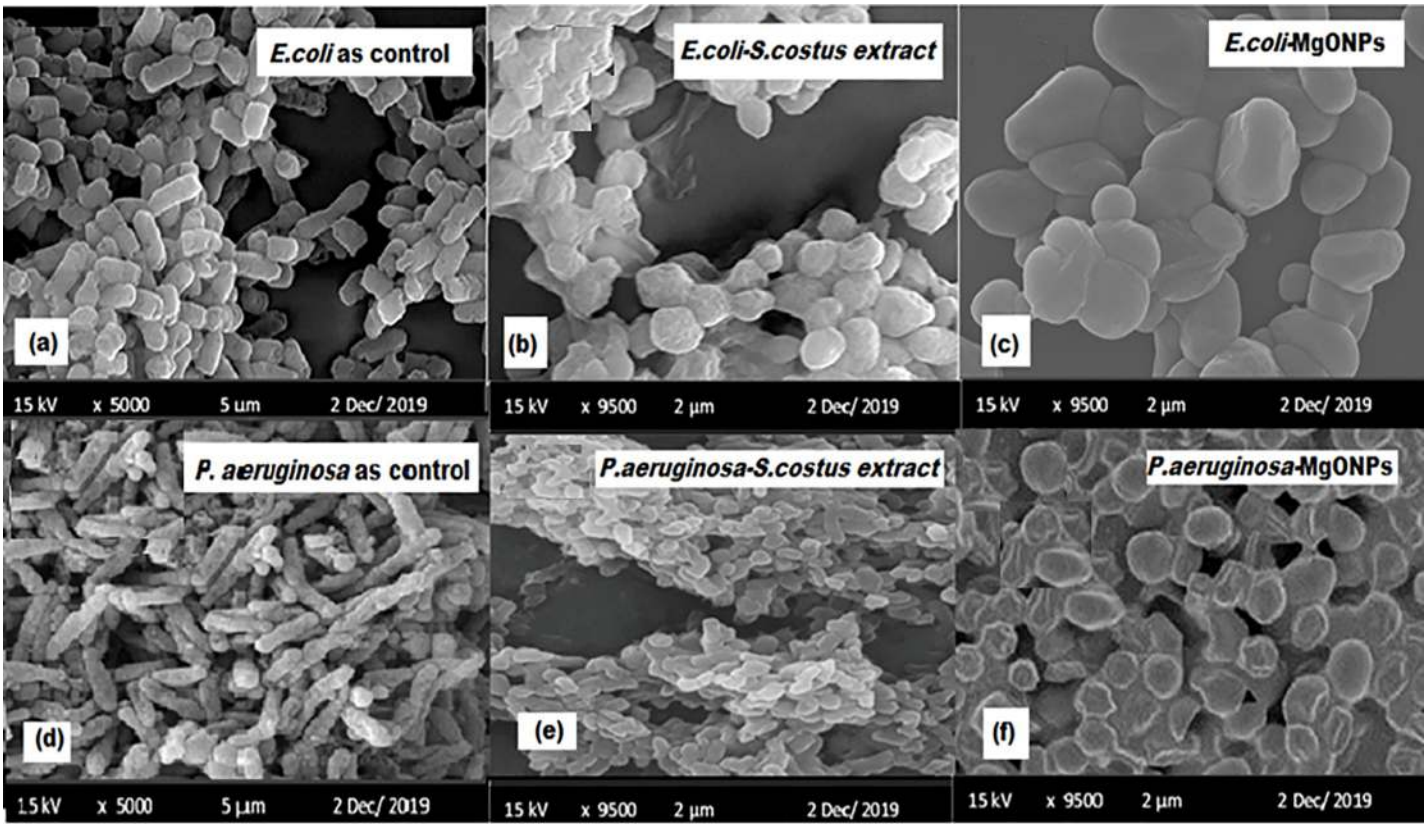

Fig 6. SEM images of untreated and treated with MgONPs (Qustal bahri) and altered shape of *E. coli* and *P. aeruginosa*.

https://doi.org/10.1371/journal.pone.0237567.g007

Antifungal activity. The prepared MgONPs were tested at three different concentrations (15, 25 and 35 µgmL^{-1}) for antifungal activity against *Candida tropicalis* ATCC 66019 and *Candida glabrata* strains. The MgONPs (Qustal hindi) showed potent antifungal activity against both fungal strains with inhibition zones 20 mm and 19 mm, respectively. However, MgONPs (Qustal hindi) displayed positive results only against *C. tropicalis* (20 mm) when compared with fluconazole as positive control (Fig 7). The antifungal effect MgONPs of could be due to the denaturation of fungal cells by penetration of MgONPs into the cell membrane and the interaction between Mg^{2+} ions with the SH- group of cell protein. Also, the oxidative stress due to the release of ROS free radicals could be the cause of fungal cell death [60].

Anticancer potential of MgONPs. In the current study, cytotoxicity of green synthesized MgONPs using two different biomasses (Qustal hindi and Qustal Bahri) was evaluated using MTT assay against breast adenocarcinoma cells (MCF-7).

Effect of MgONPs (Qustal bahri) on cell morphology. The cytotoxicity of MgONPs (Qustal bahri) on breast cancer (MCF-7) cell line was assessed by MTT and LDH assays. MTT assay was used to assess cell proliferation and cell viability with respect metabolic reduction potential of the active cell. The effect of the prepared MgONPs on MCF-7 cell viability was examined at five different concentrations (20, 40, 60, 80, and 100 µgmL^{-1}) and time intervals (12, 24, 32, 48 and 60 h), respectively. Both the biosynthesized MgONPs induced MCF-7 cell cytotoxicity in a dose dependent manner. As depicted in Fig 8A, both MgONPs inhibit the proliferation and viability of MCF-7 cancer cells as much as 5-fluorouracil does ($p<0.05$) [61]. After 48 h, IC_{50} values in MCF-7 cells were found to be 67.3% and 52.1% for MgONPs of *S. costus* (Qustal bahri) and (Qustal hindi), respectively. However, the high potential cell

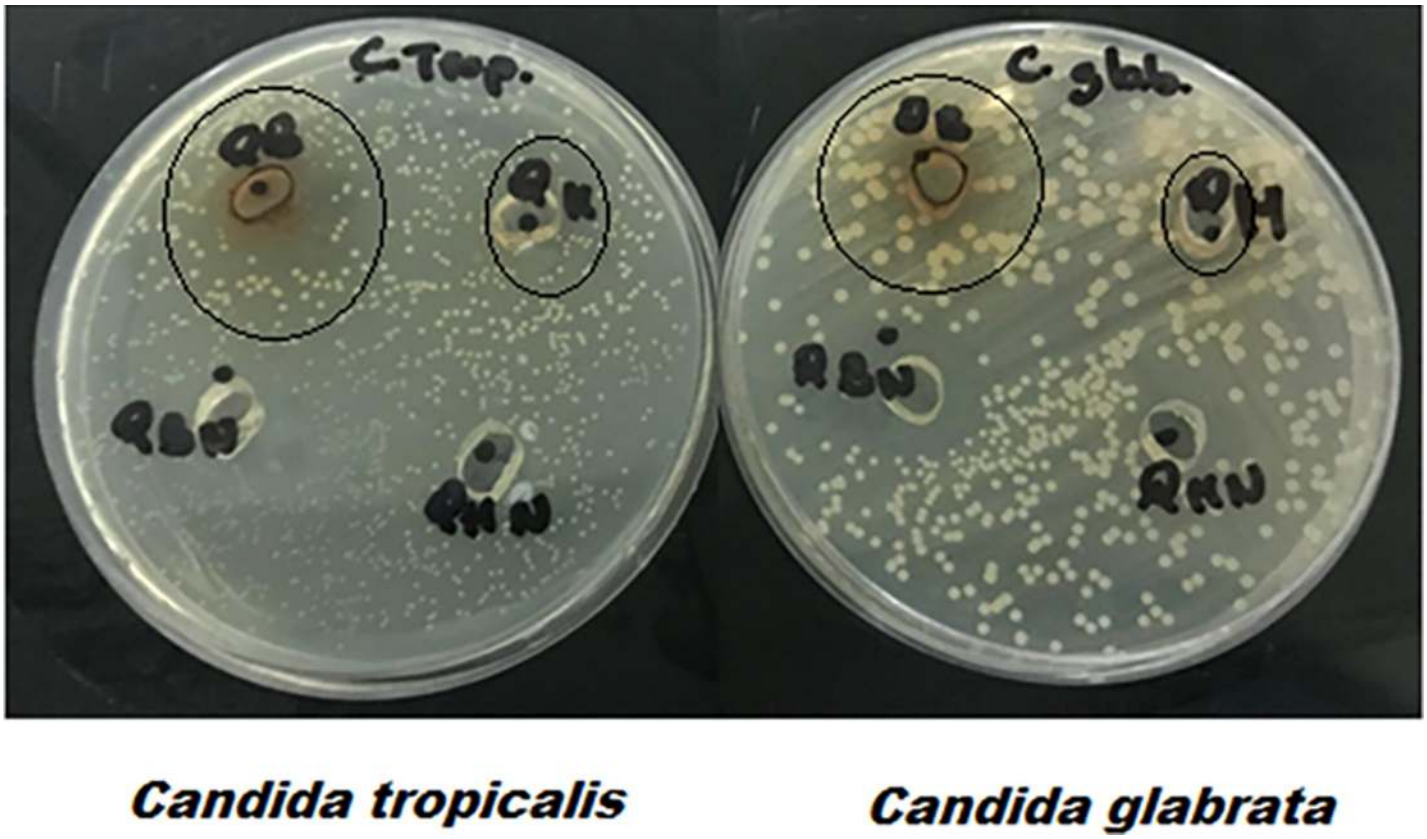

Fig 7. Antifungal activity of MgONPs synthesized by *S. costus* biomasses against *C. tropicalis* and *C. glabrata*.

https://doi.org/10.1371/journal.pone.0237567.g008

cytotoxicity was exhibited by MgONPs (Qustal bahri) as compare to the other one. The difference in the cytotoxicity is possibly related to the concentration of active constituents in the two varieties of *S.costus*. On the basis of cell cytotoxicity MgONPs (Qustal bahri) was chosen for further study. The results of microscopical analysis depicted that in the untreated group, a high cell density population with typical epithelial cell morphology was observed, whereas both treated group with MgONPs and the positive control group exhibited rounding, shrinking, membrane blebbing as well as chromatin condensation (Fig 8B). The possible mechanism of morphological changes could be attributed to cellular uptake of MgONPs by macro-pinocytosis or endocytosis and increase the production of ROS, which activated the apoptotic pathway and led to cell death (Scheme 1) [59]. To assess the cellular damage, lactate dehydrogenase (LDH) assay was used. It is a soluble cytoplasmic enzyme released into the extracellular medium during damage of cell membrane and its concentration indicates the cellular toxicity [62]. LDH assay was employed to estimate the cytotoxicity of MgONPs on the treated cells. LDH also confirms that the nanoparticles possess the cytotoxic effect again cancer cells in a dose dependent manner and resulting in cell death [62] (Fig 8C).

DNA damage and MgONPs (Qustal bahri) induced apoptosis. DNA laddering assay was used to confirm the fragmentation of DNA, which induced death in cancer cells by MgONPs. The treated cells displayed DNA laddering pattern whereas, only single DNA laddering band was obtained in the untreated cells. Moreover, the positive control group also showed DNA laddering pattern (Fig 9A). The possible apoptotic pathway is due to increase in ROS level, which leads to several pathological changes such as, DNA damage, protein oxidation, lipid peroxidation and inflammation [63]. In this study, the mechanism of the anticancer

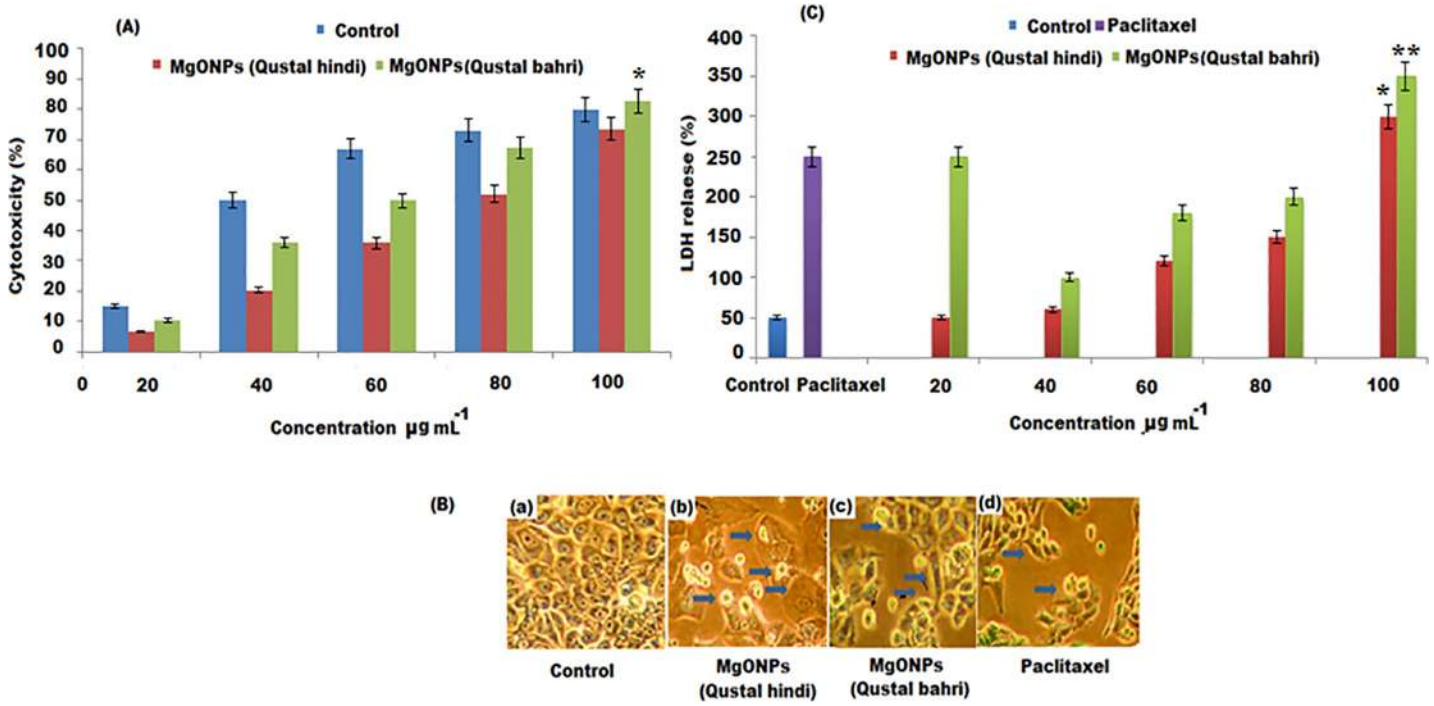

Fig 8. Anticancer effect of MgONPs on MCF-7 cells (A) MTT analysis to estimate the cytotoxicity (B) LHD assay to detect the membrane integrity and (C) microscopic images describing morphological changes.

https://doi.org/10.1371/journal.pone.0237567.g009

potential of MgONPs was assessed by studying the intracellular ROS. The outcome spectrofluorometric results demonstrated an extensive increase in fluorescence intensity in the group of cells treated with MgONPs as compared with the control group. Further investigation was

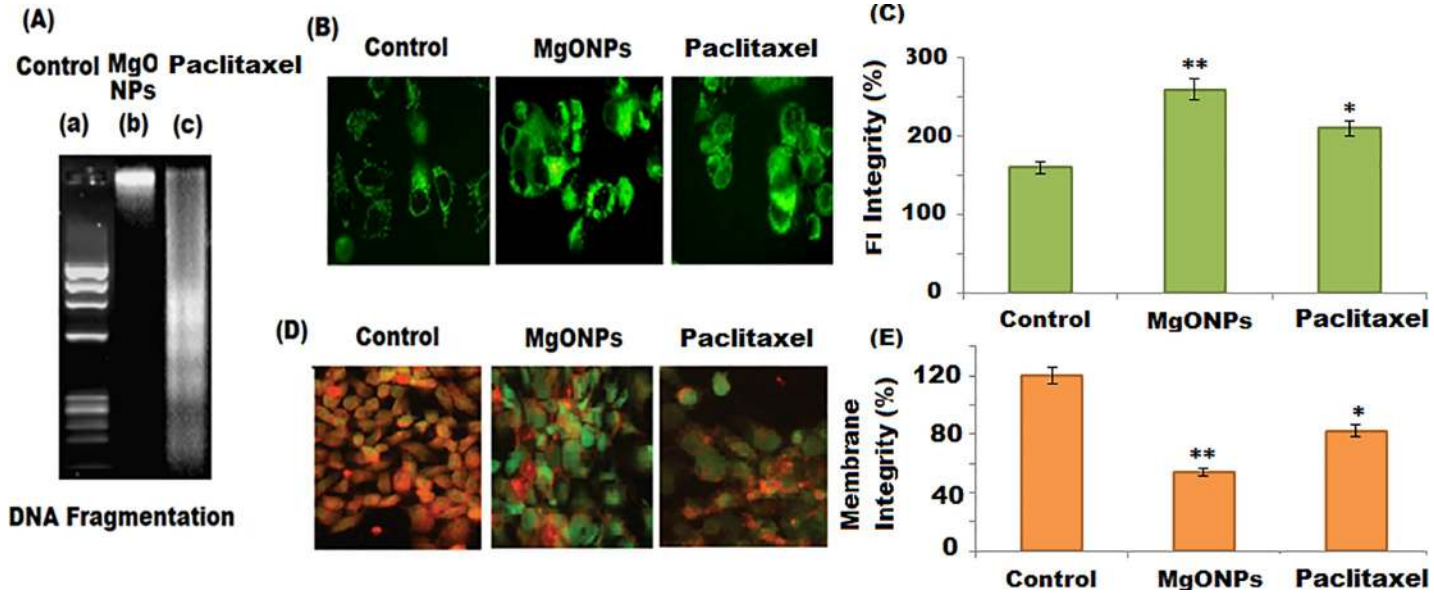

Fig 9. (A) Light microscope showing DNA fragmentation in MCF-7 cells, (B) Fluorescence microscopic images of MCF-7 cells treated with CM-H2 DCFDA, intracellular ROS indicator after treatment with MgONPs (C) quantification of ROS level using fluorescence spectroscopy, (D) Fluorescence microscopic images of MCF-7cells treated with JC-1 staining to assess the mitochondrial membrane potential ($\Delta\Psi m$) after treatment with the MgONPs for 24 h in comparison with Piacitaxel (40×) (E) Bar diagram illustrating the percentage of cells with disrupted MMP.

https://doi.org/10.1371/journal.pone.0237567.g010

carried out using fluorescence microscopic detection (Fig 9B). The treated group showed enhanced green fluorescence intensity rather than the control and positive control cells, revealing the elevation and accumulation of ROS level associated with the apoptotic effect of MgONPs on MCF-7 breast cancer cells (Fig 9C).

The Loss of mitochondrial membrane potential induced by MgONPs (Qustal bahri). Rhodamine 123 dye was used to stain the treated cells with MgONPs to evaluate the loss of membrane mitochondrial potential (MMP Ψm) in MCF-7 cancer cells. The fluorescence microscopic detection of MgONPs treated group cells showed a significant decrease in fluorescence intensity ($p < 0.05$, three fold) as compared to control group cells, indicating the disruption of MMP. The observed decrease in fluorescence intensity confirmed that MgONPs could enhance the loss in MMP (Fig 9D and 9E).

Apoptosis in MCF-7 cells induced by MgONPs (Qustal bahri). The dual staining technique was used to detect the rate of apoptosis induced by MgONPs. Double fluorescence staining acridine orange (AO) and ethidium bromide (EtBr) was used to examine the treated and untreated cell morphology under light microscope. It enables to distinguish the normal, early and late apoptotic as well as necrotic cells along with the nuclear morphology [64]. The normal and early apoptotic cells could be detected as green fluorescence by penetrating AO into the plasma membrane and binding with cell DNA. However, late apoptotic and dead cells emitted orange-red fluorescence after staining with EtBr which enter the damaged cell membrane. The obtained results showed uniformly dispersed stained green cells in the control group which indicates the presence of viable cells (Fig 10A). However, the presence of orange colored stained cells in MgONPs treated cells, indicating the presence of apoptotic cells, while as dual

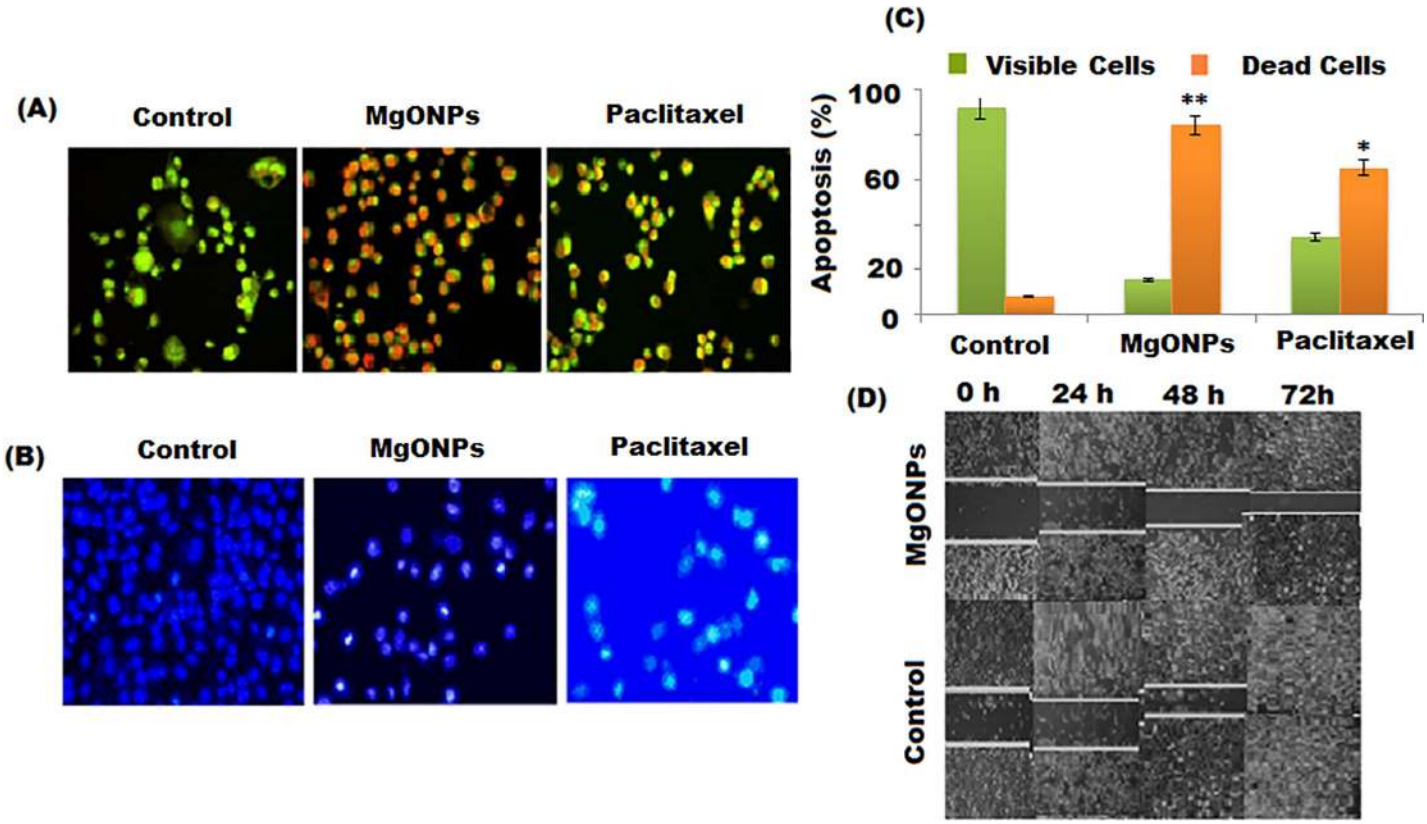

Fig 10. Antiproliferative effect of MgONPs at its IC_{50} in MCF-7 cells as depicted by (A) AO/EtBr double staining (B) quantification of apoptotic population (C) DAPI staining (D) Wound healing showing inhibition of cellular migration in MgONPs treated group of MCF-7 cells.

https://doi.org/10.1371/journal.pone.0237567.g011

stained green and orange colored were found in Paclitaxel treated cells, illustrating necrosis. The comparative results of quantitative detection demonstrated a potential increase of dead cells in MgONPs treated group (84.3 ± 0.01% dead and 15.7 ± 0.02% viable cells), (8.3 ± 0.7% dead cells and 91.8 ± 0.9 viable cells) in the control group and (65.4 ± 0.06% dead cells and 34.6 ± 0.04% viable cells) in Paclitaxel treated group (Fig 10B). Further insight to study the mode of cell death induced by MgONPs in MCF-7 cells 4′,6-diamidino-2-phenylindole (DAPI) staining was performed. The treatment of MgONPs of MCF-7 cells caused morphological alteration and chromatin condensation in the nucleus, illustrating the apoptotic effect of MgONPs depend on the production of ROS, which resulted in oxidative stress mediated cell death in MCF-7 cells (Fig 10C). The intracellular ROS level enhanced by MgONPs disrupted the MMP and caused activation of the intrinsic pathway of apoptosis leading to cell death [65].

Cellular migration and delayed wound healing effect of MgONPs. Cell migration is one of the most important key features of cancer cells which affect their spreading and metastasis. Wound scratch healing assay was used to evaluate the effect of MgONPs on cellular migration. Fig 10D showed a significant inhibition in cellular migration and delayed wound healing.

Photocatalytic effect of MgONPs. The photocatalytic properties of the green synthesized MgONPs were investigated based on their ability to degrade the organic dye such as methylene blue (MB) which is involved in various industry purposes. The optimum absorbance of MB was determined as a function of time intervals and the percentage of decolonization was calculated. The measurements were carried out at absorbance wavelength 660 nm. Fig 11 showed

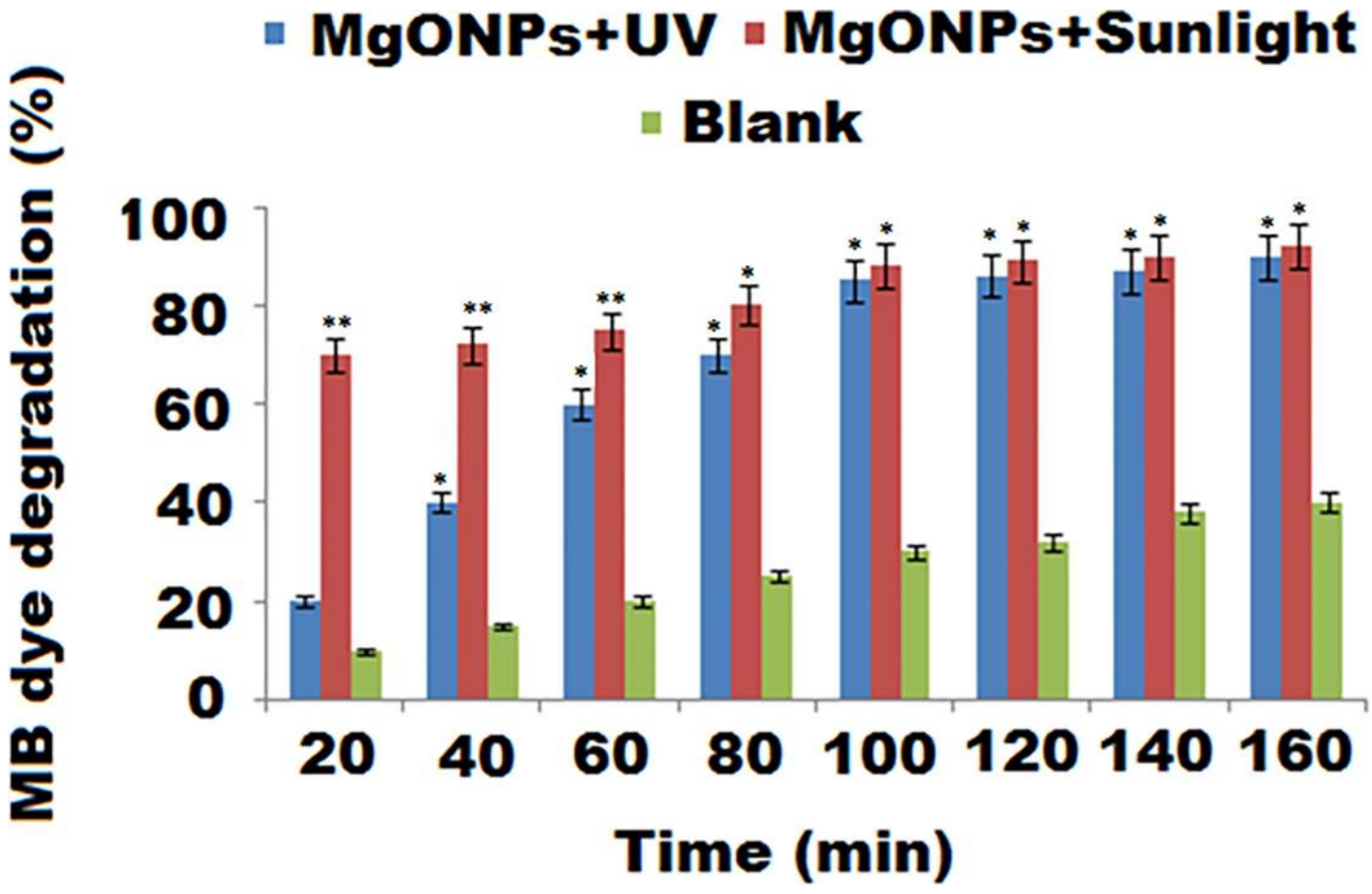

Fig 11. Catalytic effect of MgONPs calculated as % of MB dye degradation in the presence of UV radiation and sunlight.

https://doi.org/10.1371/journal.pone.0237567.g012

the degradation effect of MgONPs on MB in the presence of both UV and visible lights. It was observed that the synthesized MgONPs prepared by Qustal bahri and Qustal hindi exhibited 92% and 59% times the potent catalytic activity higher than the blank MB. The obtained results are attributed to the ability of metal oxides nanoparticles to absorb light and produce a charge separation with the formation of holes that can oxidize or reduce the organic compounds such as organic dyes [66, 67]. Similarly, the photocatalytic process of MgONPs, are due to their activation in the presence of UV or visible light and the photoexcited electrons are trasferred from the valance band to the conduction band inducing electron/hole pair (e-/h+) which responsible for the redox interaction of the adsorbed organic dye on their surface.

Conclusion

The current study described simple, clean, ecofriendly, safe and inexpensive method for the synthesis of MgONPs using two root extracts of *S. costus*. The synthesized MgONPs were subjected to different microscopic and spectroscopic investigations to ensure their nanostructures. The obtained results revealed the formation of nanoparticles with particle size of 30 and 34 nm for the MgONPs prepared using Qustal hindi and Qustal bahri, respectively. These nanoparticles were screened for antimicrobial and cytotoxicity against different pathogenic microbes as well as MCF-7 cancer cells. It was found that the nanoparticles showed improved antimicrobial and anticancer properties when compared with the biomasses of *S. costus*. Moreover, MgONPs prepared from Qustal bahri biomass exhibited better antimicrobial and anticancer potential. Also, the synthesized nanoparticles demonstrated an enhanced 92% and 59% photocatalytic degradation of methylene blue after UV irradiation for 1 h for those prepared using Qustal bahri and Qustal hindi, respectively.

Supporting information

S1 Raw images.
(PDF)

Author Contributions

Conceptualization: Musarat Amina.

Data curation: Musarat Amina.

Formal analysis: Nawal M. Al Musayeib, Nawal A. Alarfaj, Gadah A. Al Hamoud.

Methodology: Maha F. El-Tohamy, Nadine M. S. Moubayed.

Resources: Nawal M. Al Musayeib, Sarah I. Bukhari.

Validation: Maha F. El-Tohamy.

Visualization: Sarah I. Bukhari, Nadine M. S. Moubayed.

Writing – review & editing: Nawal A. Alarfaj, Hesham F. Oraby, Gadah A. Al Hamoud.

References

1. Amendola V, Pilot R, Frasconi M, Marago MO, Iati MA. Surface plasmon resonance in gold nanoparticles: a review. Journal of Physics Condensed Matter. 2017; 29: 203002. https://doi.org/10.1088/1361-648X/aa60f3 PMID: 28426435
2. Alric C, Taleb J, Duc GL, Mandon C, Billotey C, MeurHerland AL, et al. Gadolinium chelate coated gold nanoparticles as contrast agents for both X-ray computed tomography and magnetic resonance

imaging. Journal of American Chemical Society. 2008; 130: 5908–5915. https://doi.org/10.1021/ja078176p PMID: 18407638

3. Pandit S, Dasgupta D, Dewan N, Ahmed P. Nanotechnology based biosensors and its application. The Pharma Innovation Journal. 2016; 5(6): 18–25.
4. Schultz S, Smith DR, Mock JJ, Schultz DA. Single-target molecule detection with nonbleaching multicolor optical immunolabels. Proceedings of the National Academy of Sciences of the United States of America. 2000; 97: 996–1001. https://doi.org/10.1073/pnas.97.3.996 PMID: 10655473
5. Kelly KL, Coronado E, Zhao LL, Schatz CC. The optical properties of metal nanoparticles: the influence of size, shape, and dielectric environment. Journal of Physical Chemistry B. 2003; 107: 668–677. https://doi.org/10.1021/jp026731y
6. Hasan A, Morshed M, Memic A, Hassan S, Webster TJ, Mare HE. Nanoparticles in tissue engineering: applications, challenges and prospects. International Journal of Nanomedicine. 2018; 13: 5637–5655. https://doi.org/10.2147/IJN.S153758 PMID: 30288038
7. Bereka MM. Nanotechnology in food industry; advances in food processing, packaging and food Safety. International Journal of Current Microbiology and Applied Sciences. 2015; 4: 345–357.
8. Liangbing H, Cui Y. Energy and environmental nanotechnology in conductive paper and textiles. Energy & Environmental Science. 2012; 5: 6423–6435. https://doi.org/10.1039/C2EE02414D
9. Ramanujam K, Sundrarajan M. Antibacterial effects of biosynthesized MgO nanoparticles using an ethanolic fruit extract of *Emblica officinalis*. Journal of Photochemistry & Photobiology B: Biology. 2014; 141: 296–300. https://doi.org/10.1016/j.jphotobiol.2014.09.011 PMID: 25463681
10. Jain A, Wadhawan S, Kumar V, Mehta S. Colorimetric sensing of Fe^{3+} ions in aqueous solution using Magnesium oxide nanoparticles synthesized using green approach. Chemical Physics Letters. 2018; 706: 53–61. https://doi.org/10.1016/j.cplett.2018.05.069
11. Salem JK, El-Nahhal IM, Hammad TM, Kuhn S, Sharekh SA, El-Askalani M, et al. Optical and fluorescence properties of MgO nanoparticles in micellar solution of hydroxyethyl laurdimonium chloride. Chemical Physics Letters. 2015; 636: 26–30. https://doi.org/10.1016/j.cplctt.2015.07.014
12. Mangalampalli B, Dumala N and Grover P. Allium cepa root tip assay in assessment of toxicity of magnesium oxide nanoparticles and microparticles. Journal of Environmental Sciences. 2018; 66: 125–137. https://doi.org/10.1016/j.jes.2017.05.012 PMID: 29628079
13. Umaralikhan L, Jaffar MJ. Green synthesis of MgO nanoparticles and it antibacterial activity. Iranian Journal of Science and Technology, Transactions A: Science. 2018; 42(2): 477–485. http://dx.doi.org/10.1007/s40995-016-0041-8
14. Adil SF, Assal ME, Khan M, Al-Warthan A, Siddiqui MR, Liz-Marzán LM. Biogenic synthesis of metallic nanoparticles and prospects toward green chemistry. Dalton Transactions. 2015; 44(21): 9709–9717. https://doi.org/10.1039/c4dt03222e PMID: 25633046
15. Li Z, Yang T. The application of Biomolecules in the Preparation of Nanomaterials. Biomedical Engineering: Frontiers and Challenges. 2011: 319.
16. Butola JS, Samant SS. Saussurea species in Indian Himalayan Region: diversity, distribution and indigenous uses. International Journal of Plant Biology. 2010; 1: 43–51. https://doi.org/10.4081/pb.2010.e9
17. Amara U, Mashwani Z, Khan A, Laraib S, Wali R, Sarwar U, et al. Conservation status and therapeutic potential of *Saussurea lappa*: An Overview. American Journal of Plant Science 2017; 8: 602–614.
18. Madhuri K, Elango K, Ponnusankar S. *Saussurea lappa* (Kuth root): review of its traditional uses, phytochemistry and pharmacology. Oriental Pharmacy and Experimental Medicine. 2012; 12: 1–9. https://doi.org/10.1007/s13596-011-0043-1
19. Hasson SS, Al-Balushi MS, Al-Busaidi J, Othman MS, Said EA, Habal O, et al. Evaluation of anti–resistant activity of Auklandia (*Saussurea lappa*) root against some human pathogens. Asian Pacific Journal of Tropical Biomedicine. 2013; 3(7): 557–562. https://doi.org/10.1016/S2221-1691(13)60113-6 PMID: 23836413
20. Tian X, Song HS, Cho YM, Park B, Song YJ, Jang S, et al. Anticancer effect of *Saussurea lappa* extract via dual control of apoptosis and autophagy in prostate cancer cells. Medicine. 2017; 96(30): e7606. https://doi.org/10.1097/MD.0000000000007606 PMID: 28746210
21. Eliza J, Daisy P, Ignacimuthu S, Duraipandiyan V. Antidiabetic and antilipidemic effect of eremanthin from Costus speciosus (Koen.) Sm., in STZ-induced diabetic rats. Chemico-biological Interactions. 2009; 182(1): 67–72. https://doi.org/10.1016/j.cbi.2009.08.012 PMID: 19695236
22. Alnahdi HS, Ayaz NO, Elhalwagy ME. Prophylactic effect of cousts *saussurea lappa* against liver injury induced by deltamethrin intoxication. International Journal of Clinical Experimental and Pathology 2016; 9(1): 387–394.
23. Tag HM, Khaled HE, Ismail HA, El-Shenawy NS. Evaluation of anti-inflammatory potential of the ethanolic extract of the *Saussurea lappa* root (costus) on adjuvant-induced monoarthritis in rats. Journal of

basic and clinical physiology and pharmacology. 2016; 27(1): 71–78. https://doi.org/10.1515/jbcpp-2015-0044 PMID: 26479340

24. Singh R, Chahal KK, Singla N. Chemical composition and pharmacological activities of *Saussurea lappa*: A review. Journal of Pharmacognsy & Phytochemistry. 2017; 6: 1298–1308.
25. Mangalampalli B, Dumala N, Grover P. Acute oral toxicity study of magnesium oxide nanoparticles and microparticles in female albino Wistar rats. Regulatory Toxicology and Pharmacology. 2017; 90: 170–184. https://doi.org/10.1016/j.yrtph.2017.09.005 PMID: 28899817
26. De Silva RT, Mantilaka MM, Goh KL, Ratnayake SP, Amaratunga GA, de Silva KM. Magnesium oxide nanoparticles reinforced electrospun alginate-based nanofibrous scaffolds with improved physical properties. International Journal of Biomaterials. 2017; 2017. https://doi.org/10.1155/2017/1391298
27. He Y, Ingudam S, Reed S, Gehring A, Strobaugh TP, Irwin P. Study on the mechanism of antibacterial action of magnesium oxide nanoparticles against food borne pathogens. Journal of Nanobiotechnology. 2016; 14: 54. https://doi.org/10.1186/s12951-016-0202-0 PMID: 27349516
28. Nguyen NY, Grelling N, Wetteland CL, Rosario R, Liu H. Antimicrobial activities and mechanisms of magnesium oxide nanoparticles (nMgO) against pathogenic bacteria, yeasts, and biofilms. Scientific reports. 2018; 8(1): 1–23. https://doi.org/10.1038/s41598-017-17765-5
29. Akhtar MJ, Ahamed M, Alhadlaq HA, Alrokayan SA. MgO nanoparticles cytotoxicity caused primarily by GSH depletion in human lung epithelial cells. Journal of Trace Elements in Medicine and Biology. 2018; 50: 283–90. https://doi.org/10.1016/j.jtemb.2018.07.016 PMID: 30262293
30. Pugazhendhi A, Prabhu R, Muruganantham K, Shanmuganathan R, Natarajan S. Anticancer, antimicrobial and photocatalytic activities of green synthesized magnesium oxide nanoparticles (MgONPs) using aqueous extract of Sargassum wightii. Journal of Photochemistry and Photobiology B: Biology. 2019; 190: 86–97. https://doi.org/10.1016/j.jphotobiol.2018.11.014 PMID: 30504053
31. De Hoon JP, Veeck J, Vriens BE, Calon TG, van Engeland M, Tjan-Heijnen VC. Taxane resistance in breast cancer: A closed HER2 circuit. Biochimica et Biophysica Acta. 2012; 1825: 197–206. https://doi.org/10.1016/j.bbcan.2012.01.001 PMID: 22280939
32. Mansoori B, Mohammad A, Davudian S, Shirjang S, Baradaran B. The Different Mechanisms of Cancer Drug Resistance: A Brief Review. Advanced Pharmaceutical Bulletin. 2017; 7: 339–348. https://doi.org/10.15171/apb.2017.041 PMID: 29071215
33. Seigneuric R, Markey L, Nuyten DSA, Dubernet C, Evelo CTA, Finot E, et al. From nanotechnology to nanomedicine: applications to cancer research. Current Molecular Medicine. 2010; 10: 640–652. https://doi.org/10.2174/156652410792630634 PMID: 20712588
34. Sharma A, Goyal AK, Rath G. Recent advances in metal nanoparticles in cancer therapy. Journal of Drug Targeting. 2018; 26: 617–632. https://doi.org/10.1080/1061186X.2017.1400553 PMID: 29095640
35. Behzadi E, Sarsharzadeh R, Nouri M, Attar F, Akhtari K, Shahpasand K, et al. Albumin binding and anticancer effect of magnesium oxide nanoparticles. International Journal of Nanomedicine. 2019; 14: 257–270. https://doi.org/10.2147/IJN.S186428 PMID: 30643405
36. Sudakaran SV, Venugopal JR, Puvala G. Sequel of MgO nanoparticles in PLACL nanofibers for anticancer therapy in synergy with curcumin/β-cyclodextrin. Materials Science and Engneering. 2017; C71: 620–628. https://doi.org/10.1016/j.msec.2016.10.050 PMID: 27987753
37. Berghe VA, Vlietinek AJ. Screening methods for antibacterial and antiviral agents from higher plants. Methods in Plant Biochemistry. 1991; 6: 47–48. https://hdl.handle.net/10067/8870151162165141.
38. Patel DK, Singh RK, Singh SK, Aswal VK, Rana D, Ray B, et al. Graphene as a chain extender of polyurethanes for biomedical applications. RSC Advances. 2016; 6: 58628–40. https://doi.org/10.1039/C6RA12792D.
39. Patere SN, Pathak PO, Shukla AK, Singh RK, Dubey VK, Mehta MJ, et al. Surface-modified liposomal formulation of amphotericin B: in vitro evaluation of potential against visceral leishmaniasis. AAPS PharmSciTech. 2017; 18: 710–20. https://doi.org/10.1208/s12249-016-0553-8 PMID: 27222025
40. Chan FK, Moriwaki K, De Rosa MJ. Detection of necrosis by release of lactate dehydrogenase activity. Methods in Molecular Biology. 2013; 979: 65–70. https://doi.org/10.1007/978-1-62703-290-2_7 PMID: 23397389
41. Lautraite S, Bigot-Lasserre D, Bars R, Carmichael N. Optimization of cell-based assays for medium throughput screening of oxidative stress. Toxicology in vitro. 2003; 17: 207–220. https://doi.org/10.1016/s0887-2333(03)00005-5 PMID: 12650675
42. Suganthy N, Devi KP. Protective effect of catechin rich extract of *Rhizophora mucronata* against β-amyloid-induced toxicity in PC12 cells. Journal of Applied Biomedicine. 2016; 14: 137–146. https://doi.org/10.1016/j.jab.2015.10.003

43. Gupta S, Prasad GVRK, Mukhopadhaya A.Vibrio cholerae porin OmpU induces caspase-independent programmed cell death upon translocation to the host cell mitochondria. Journal of Biological Chemistry. 2015; 290: 31051–31068. https://doi.org/10.1074/jbc.M115.670182 PMID: 26559970

44. Pugazhendhi A, Prabhu R, Muruganantham K, Shanmuganathan R, Natarajan S. Anticancer, antimicrobial and photocatalytic activities of green synthesized magnesium oxide nanoparticles (MgONPs) using an aqueous extract of Sargassum wightii. Journal of Photochemistry and Photobiology B: Biology. 2019; 190:86–97. https://doi.org/10.1016/j.jphotobiol.2018.11.014 PMID: 30504053

45. Singh M, Singh RK, Singh SK, Mahto SK, Misra N. In vitro biocompatibility analysis of functionalized poly (vinyl chloride)/layered double hydroxide nanocomposites. RSC Advances. 2018; 8: 40611–40620. https://doi.org/10.1039/C8RA06175K.

46. Alam F, Najum Q, Waheed A. Cytotoxic activity of extracts and crude saponins from Zanthoxylum armatum DC. against human breast (MCF-7, MDA-MB-468) and colorectal (Caco-2) cancer cell lines. BMC Complementary and Alternative Medicine. 2017; 17: 368. https://doi.org/10.1186/s12906-017-1882-1 PMID: 28716103

47. Mirza MB, Elkady AI, Al-Attar AM, Syed FQ, Mohammed FA, Hakeem KR. Induction of apoptosis and cell cycle arrest by ethyl acetate fraction of Phoenix dactylifera L.(Ajwa dates) in prostate cancer cells. Journal of Ethnopharmacology. 2018; 218: 35–44. https://doi.org/10.1016/j.jep.2018.02.030 PMID: 29476962

48. Nikseresht M, Kamali A, Rahimi H, Delaviz H, Toori M, Kashani I, et al. The hydroalcoholic extract of Matricaria chamomilla suppresses migration and invasion of human breast cancer MDA-MB-468 and MCF-7 cell lines. Pharmacognosy Research. 2017; 9: 87–95. https://doi.org/10.4103/0974-8490.199778 PMID: 28250660

49. Fedlheim DL, Foss CA. Metal nanoparticles: synthesis, characterization, and applications. CRC press; 2001 Oct 26.

50. Jeevanandam J, San Chan Y, Danquah MK. Biosynthesis and characterization of MgO nanoparticles from plant extracts via induced molecular nucleation. New Journal of Chemistry. 2017; 41(7): 2800–2814. https://doi.org/10.1039/C6NJ03176E.

51. Nakamoto K. Infrared and Raman spectra of inorganic and coordination compounds, Handbook of vibrational spectroscopy, 2006.

52. Sharma G, Soni R, Jasuja ND. Phytoassisted synthesis of magnesium oxide nanoparticles with Swertia chirayaita. Journal of Taibah University for Science. 2017; 11: 471–477. https://doi.org/10.1016/j.jtusci.2016.09.004.

53. Schamps J, Gandara G. A 3Δ-3Π transition in the near-ultraviolet spectrum of MgO. Journal of Molecular Spectroscopy. 1976; 62(1): 80–84.https://doi.org/10.1016/00222852(76)90264-2

54. Camtakan Z, Erenturk S, Yusan S. Magnesium oxide nanoparticles: preparation, characterization, and uranium sorption properties. Environmental Progress & Sustainable Energy. 2012; 31(4): 536–543. https://doi.org/10.1002/ep.10575.

55. Samodi A, Rashidi A, Marjani K, Ketabi S. Effects of surfactants, solvents and time on the morphology of MgO nanoparticles prepared by the wet chemical method. Materials Letters. 2013; 109: 269–274. https://doi.org/10.1016/j.matlet.2013.07.085

56. Srivastava V, Sharma YC, Sillanpa M. Green synthesis of magnesium oxide nanoflower and its application for the removal of divalentmetallic species from synthetic wastewater. Ceramics International. 2015; 41: 6702–6709. https://doi.org/10.1016/j.ceramint.2015.01.112

57. Rezaei M, Khajenoori M, Nematollahi B. Synthesis of high surface area nanocrystalline MgO by pluronic P123 triblock copolymer surfactant. Powder Technology. 2011; 205: 112–116.

58. Krishnamoorthy K, Manivannan G, Kim SJ, Jeyasubramanian K, Premanathan M. Antibacterial activity of MgO nanoparticles based on lipid peroxidation by oxygen vacancy. Journal of Nanoparticle Research. 2012; 14: 1063. https://doi.org/10.1007/s11051-012-1063-6.

59. Verma SK, Jha E, Panda PK, Thirumurugan A, Suar M. Biological Effects of Green-Synthesized Metal Nanoparticles: A Mechanistic View of Antibacterial Activity and Cytotoxicity. InAdvanced Nanostructured Materials for Environmental Remediation 2019 (pp. 145–171). Springer, Cham. https://doi.org/10.1007/978-3-030-04477-0-6.

60. Sierra-Fernandez A, De la Rosa-Garcia S, Gomez-Villalba LS, Gomez-Cornelio S, Rabanal ME, Fort R, et al. Synthesis, photocatalytic, and antifungal properties of MgO, ZnO and Zn/Mg oxide nanoparticles for the protection of calcareous stone heritage. ACS Applied Materials and Interfaces. 2017; 9: 24873–24886. https://doi.org/10.1021/acsami.7b06130 PMID: 28679041

61. Gunduz N, Ceylan H, Guler MO, Tekinay AB. Intracellular accumulation of gold nanoparticles leads to inhibition of macropinocytosis to reduce the endoplasmic reticulum stress. Scientific Reports. 2017; 7: 40493. https://doi.org/10.1038/srep40493 PMID: 28145529

62. Smith SM, Wunder MB, Norris DA, Shellman YG. A simple protocol for using a LDH-based cytotoxicity assay to assess the effects of death and growth inhibition at the same time. PloS one. 2011; 6: e26908. https://doi.org/10.1371/journal.pone.0026908 PMID: 22125603

63. Liou G-Y, Storz P. Reactive oxygen species in cancer. Free Radical Research. 2010; 44: 479–496. https://doi.org/10.3109/10715761003667554 PMID: 20370557

64. Kumar S, Sharma VK, Yadav S, Dey S. Antiproliferative and apoptotic effects of black turtle bean extracts on human breast cancer cell line through extrinsic and intrinsic pathway. Chemistry Central Journal. 2017; 11: 56. https://doi.org/10.1186/s13065-017-0281-5 PMID: 29086840

65. Verma SK, Nisha K, Panda PK, Patel P, Kumari P, Mallick MA, et al. Green synthesized MgO nanoparticles infer biocompatibility by reducing in vivo molecular nanotoxicity in embryonic zebrafish through arginine interaction elicited apoptosis. Science of The Total Environment. 2020; 713: 136521. https://doi.org/10.1016/j.scitotenv.2020.136521 PMID: 31951838

66. Hisatomi T, Kubota J, Domen K. Recent advances in semiconductors for photocatalytic and photoelectrochemical water splitting. Chemical Society Reviews. 2014; 43(22):7520–7535. https://doi.org/10.1039/c3cs60378d PMID: 24413305

67. Hoffmann MR, Martin ST, Choi W, Bahnemann DW. Environmental applications of semiconductor photocatalysis. Chemical reviews. 1995; 95(1): 69–96. https://doi.org/10.1021/cr00033a004